TECHNISCHE UNIVERSITÄT WIEN
Vienna | Austria

Diploma Thesis

# Modelling of time-temperature shifts of viscoelastic composites

carried out for the purpose of obtaining the degree of

Diplom-Ingenieur

submitted at TU Wien, Faculty of Mechanical and Industrial Engineering,

by

**Lukas Huber**, BSc

Matr.Nr.: 01426099

under the supervision of

Associate Prof. Dipl.-Ing. Dr.techn. **Heinz Pettermann**

Assistant Prof. Dipl.-Ing. Dr.techn. **Melanie Todt**

Institute of Lightweight Design and Structural Biomechanics (E317)

Vienna, September 2020

I confirm, that going to press of this thesis needs the confirmation of the examination committee.

*Affidavit*

I declare in lieu of oath, that I wrote this thesis and performed the associated research myself, using only literature cited in this volume. If text passages from sources are used literally, they are marked as such. I confirm that this work is original and has not been submitted elsewhere for any examination, nor is it currently under consideration for a thesis elsewhere.

*City and Date* *Signature*

# Acknowledgement

First and foremost, I would like to express my deepest appreciation to my supervisor Prof. Heinz Pettermann of the Institute of Lightweight Design and Structural Biomechanics at TU Vienna for his consistent support and guidance. I am also very grateful for his useful feedback and valuable comments on my thesis.

I would like to thank senior scientist Dr Thomas Koch of the Institute of Materials Science and Technology at TU Vienna for providing me measured material data.

Also, I gratefully acknowledge the ILSB itself for the supply of needed hard- and software. Special thanks are directed to IT-manager Gerhard Schneider who took care of every occurring IT problem and setup a remote access to the ILSB system.

Finally, I wish to thank my parents Inge and Friedrich Huber for their continues love, support and encouragement since my childhood. I am eternally grateful to my deceased grandfather, Alois Roithinger, without whom I would never have got fascinated about technology.

# Abstract

The present master thesis addresses the relaxation and the time-temperature behaviour of a viscoelastic unidirectional composite, which consists of two different viscoelastic components. The aim of this work is to determine the effective relaxation behaviour and the time-temperature behaviour of this unidirectional composite. Therefore the periodic microfield approach, which is a common method in the micromechanic of materials, is used as a meshed unit cell to numerically determine the relaxation behaviour at different temperatures. The parameters of the shifting functions are determined by trial and error.

The results of the composite's relaxation behaviour show that the fibre itself dominates in fibre direction for the majority whereas the matrix dominates the behaviour transverse the fibre direction as well as the shear behaviour. The corresponding time-temperature behaviour is in general thermorheoligically complex but two individually fitted shifts state a kind of direction-wise thermorheologically simple behaviour. Therefore the assumption of a direction dependent thermorheoligically simple composite is acceptable for a small temperature range.

A comparison between the Williams-Landel-Ferry- and the Arrhenius shifting parameters of the pure fibre, pure matrix and the determined ones of the composite shows a dominance of the matrix on the composite's overall time-temperature behaviour. The big difference between the Arrhenius shifting parameters of fibre and matrix causes such a behaviour. A change of the fibre's shifting parameters leads to new relations for the overall time-temperature behaviour as well as to more apparent changes of curvature in the relaxation development. The time-temperature behaviours of typical matrix dominated load cases are still dominated by the matrix.

# Kurzfassung

Die vorliegende Masterarbeit befasst sich mit dem Relaxations- und dem Zeit-Temperatur Verhalten eines viskoelastischen unidirektionalen Verbundwerkstoffes, welcher aus zwei unterschiedlichen viskoelastischen Komponenten besteht. Das Ziel dieser Arbeit ist es, das effektive Relaxationsverhalten und das Zeit-Temperatur Verhalten dieses unidirektionalen Verbundwerkstofes zu bestimmen. Dazu wird ein Periodic Microfield Approach, eine gängige Methode der Mikromechanik von Materialien in Form einer Einheitszelle herangezogen, um damit das Relaxationsverhalten bei verschiedenen Temperaturen numerisch zu ermitteln. Die Parameter der Verschiebungsfunktionen werden manuell bestimmt.

Die Ergebnisse zeigen, dass das Relaxationsverhalten des Verbundwerkstoffes von der Faser in Faserrichtung zum Großteil durch ihre Eigenschaften dominiert wird, während die Matrix das Verhalten quer zur Faserrichtung und auch das Schubverhalten dominiert. Das zugehörige Zeit-Temperatur Verhalten ist im Allgemeinen thermorheologisch komplex, aber mit zwei unabhängig angepassten Verschiebungsfunktionen lässt sich ein annähernd richtungsabhängiges thermorheologisch einfaches Verhalten zeigen. Darum ist die Annahme eines richtungsabhängigen thermorheologisch einfachen Verbundwerkstoffes für einen kleinen Temperaturbereich zulässig.

Ein Vergleich der Parameter der Williams-Landel-Ferry- und Arrhenius-Verschiebungsfunktionen zwischen der reinen Faser, reinen Matrix und die Ermittelten des Verbundwerkstoffes zeigt eine Dominanz der Matrix gegenüber des globalen Zeit-Temperatur Verhaltens des Verbundwerkstoffes. Ein solches Verhalten wird durch den großen Unterschied zwischen den Arrhenius Verschiebungsparametern von der Faser und der Matrix verursacht. Eine Veränderung der Verschiebungsparameter der Faser führt zu neuen Verhältnissen im globalen Zeit-Temperatur-Verhalten sowie zu deutlicheren Krümmungsänderungen in den Relaxationsverläufen. Das Zeit-Temperatur Verhalten wird für die typischen Matrix dominierten Lastfälle immer noch von der Matrix dominiert.

# Contents

# Chapter 1

# General Introduction

## 1.1 Polymers

The first plastic materials already appeared in the 18$^{th}$ century which are tree saps known as natural rubber but also the first synthetic plastics like celluloid appeared in the mid of the 19$^{th}$ century. Since the mid of the 20$^{th}$ plastics have been researched in respect of their material properties especially the mechanical ones due to a higher focus in terms of lightweight design.

### 1.1.1 Polymer structure

Plastics consist of an accumulation of macromolecular organic chains which are build together by repeating units of molecules segments, the so called monomers. In those chains there are more than 1000 bounded atoms and adding or removing an additional monomer to the chain does not change the polymer properties significantly [13]. The microstructure of macromolecules is described by the *constitution*, *configuration* and *conformation* [14]. The constitution of a polymer includes the chemical structure of molecules, type and sequences of the chain atoms, end groups and the length and type of branches. The spatial arrangement of single and atom groups with unchanged constitution is described by the configuration. The conformation describes the spatial shape with the same configuration by twisting or folding against the bond axis. A more detailed explanation can be seen in e.g. [14], [31] .

When monomers are successively added together a linear polymer chain arises. Entanglements can easily occur due to the circumstance of multiple existing single chains and their wild orientations. In general the polymer chains do not occur only in a linear form. When side chains are attached to their molecular backbone the polymer is called *branched* and their positions are described by their *tacticity*. When the side chains are arranged on the same side they are called *isotactic*. An alternating and periodic arrangement of

the side chains is called *syndiotactic* and the non-periodic one is called *atactic* [14]. The figure 1.1 shows an example of the possible formations of a polystyrene. It is also possible that two or more chains are chemically or physically bonded which leads to a network structure and is called *cross-linked* [19]. The figure 1.2 shows schematic examples of a linear, branched and cross-linked arrangement of macromolecular polymer chains. An energetic favourable arrangement of the polymer chains can be obtained by the *trans* or *gauche* position of the backbone which results in a helix structure of the entire chain and it is referred to e.g. [37], [13] for a more detailed explanation. The figure 1.3 shows an example of the mentioned trans and gauche position.

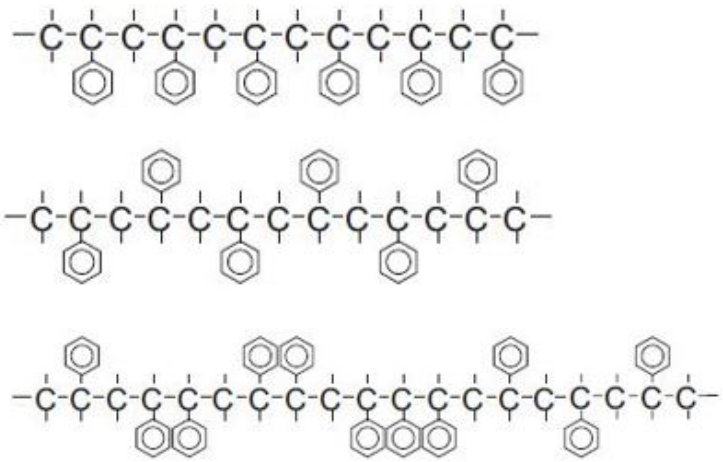

**Fig. 1.1:** The top, middle and bottom figure show an isotactic, syndiotactic and atactic polystyrene respectively where the C-atoms build up the backbone and the hexagons symbolize side chains [14]

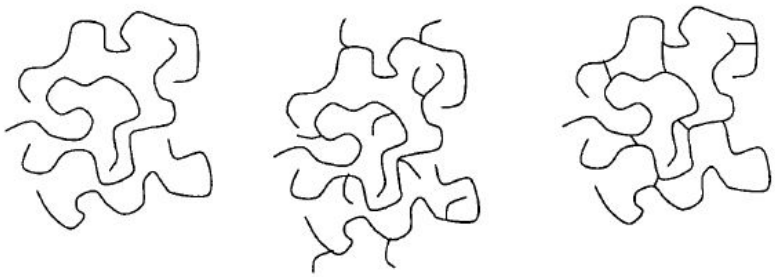

**Fig. 1.2:** The left, middle and right figure show schcematic figures of a linear, branched and cross-linked chain type respectively[19]

When a polymer chain only consists of one monomer type it is called *homopolymer*. It is also possible that the polymer chains consist of multiple different monomers which is

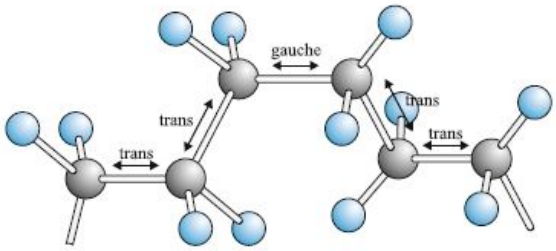


**Fig. 1.3:** The grey spheres symbolize carbon atoms and the blue ones hydrogen atoms. The polyethylene molecule can contain the trans and also the gauche conformation. In the trans state the hydrogen atoms are in staggered position of the ones from the neighbouring C-atom and in the gauche state the hydrogen atoms are either intermediate to the staggered or in the eclipsed position [5].

then called *co-polymer*. The different monomers can either be arranged alternating, block by block, sequential or in a statistical manner in the main chain but they can also be separated into main and side chain.

### 1.1.2 Classification of polymers

Polymers can be easily classified although there are numerous amounts of different polymer structures. The classification results from the pre-described structure of polymers to the categories of *thermoplasts*, *elastomers* and *thermosets*. The polymer chains in thermoplasts are arranged either in a random distribution with entanglements, the *amorphous* state, or in partial regulated arrangements, the *semi-crystalline* state. The degree of crystallinity depends generally on the constitution, configuration and conformation of the polymer chains [14]. A schematic example of a semi-crystalline polymer is displayed in figure 1.4.

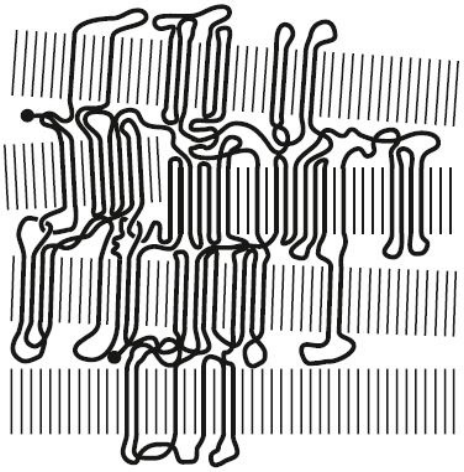

**Fig. 1.4:** Macromolecule of a schematic semi-crystalline polyethylene arranged between multiple crystalline fins and amorphous intermediate ranges [14]

An elastomer is a rubbery-like polymer which consists of sparsely cross-linked polymer chains. Those cross-links create a wide-meshed network which has a degree of cross-linking of about one cross-link per 1000 atoms. Such a kind of network enables the high deformability of elastomers. They can be distinguished between *unsaturated* elastomers who have double bonds in their polymer chains and *saturated* ones who do not have any double bonds in their chains [14]. The figure 1.5 shows a schematic example of a wide-meshed polymer chain network. A special case of the elastomers and thermoplasts are thermoplastic elastomers. Those are basically thermoplasts that have a similar material behaviour as an elastomer due to their macromolecular structure but also the ability to be deformed and shaped under temperature like a pure thermoplast [14].

Thermosets are obtained by a chemical reaction between a resin and its curing agent. Contrary to thermoplasts and elastomers thermosets are available as monomers in a liquid state and they only react with their curing agent to a solid body. After the curing process the solidified body consists of a chemical bonded and close-meshed network. The degree of

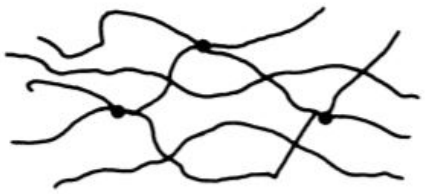

**Fig. 1.5:** The chain molecules of an schematic elastomer are strongly bonded in a wide-meshed network. A displacement of the chains itself is not possible but an elongation between the cross-links is feasible which leads to the elastic behaviour [45].

cross-links is about one cross-link per 20 atoms. A schematic representation of a thermoset is displayed in figure 1.6. A thermoset can not be liquefied any more due to the strong chemical bonds and thus they start degrading at high temperatures [14].

**Fig. 1.6:** The chain molecules of a thermoset are closer bonded and have got a higher cross-link density than an elastomer. Those chains are not able to move against each other under a thermal load [45].

### 1.1.3 Regions of polymers

Polymers show different characteristics which are dependent on temperature and are called *ranges of state*. The ranges of state describe the material property of substances over a large temperature region in respect of treatment and application. Polymers are supposed to have four [39] or five [5] different ranges of state. These regions of [5] are

- Glassy
- Transition
- Rubbery plateau

- Rubbery flow
- Liquid flow

and are displayed in figure 1.7 which shows the regions of a crystalline (A), lightly cross-linked (B) and an amorphous polystyrene (C). The ten second relaxation modulus of the amorphous polystyrene strongly decreases at a specific temperature, the *glass transition temperature* $T_g$ which is also the boundary between the glassy and the transition region. The glass transition temperature depends on some factors like the mentioned polymer structure, molecular weight, cross-linking and also intermolecular forces [32]. In the glassy region polymer chains are considered to be frozen and the deformations can only result from changes of intermolecular molecule sections or from changes of valence bond angles. A relocation of those molecule sections, a rotation of the C-C bonds or a sliding of the entanglements are not possible [14].

In the transition state the amorphous and the crystalline phase act differently. The amorphous phase regains the former restricted movements of the polymer chains whereas the crystalline phase remains unaffected because they are not able to soften. The material parameter of a semi-crystalline polymer is mostly controlled by the crystalline phase in the transition state and therefore the effects do not have such an impact as for a pure amorphous polymer [14]. A lightly cross-linked polymer acts in the glassy and also in the transition state similar to the pure amorphous one.

When the temperature is increased the transition region is left and the polymer reaches its rubbery state. Like in the transition region the behaviour of semi-crystalline polymers has to be distinguished between the amorphous phase and the crystalline one. In the amorphous phase the polymer chains gain the possibility to slide against each other which results in a smooth transition from the rubbery flow to the flow region. The polymer is considered to be liquid in this region. The crystalline phase does not soften but the crystalline structures start to dissolve and it acts more and more like the amorphous phase. The labelling temperature in the flow region is the melting temperature $T_m$. Cross-linked polymers remain unchanged in their properties after the transition region due to the cross-links which hinder a chain sliding. Furthermore the flow region of cross-linked polymers does not exist due to the fact that degradation occurs before the chemical bonds can be dissolved [39].

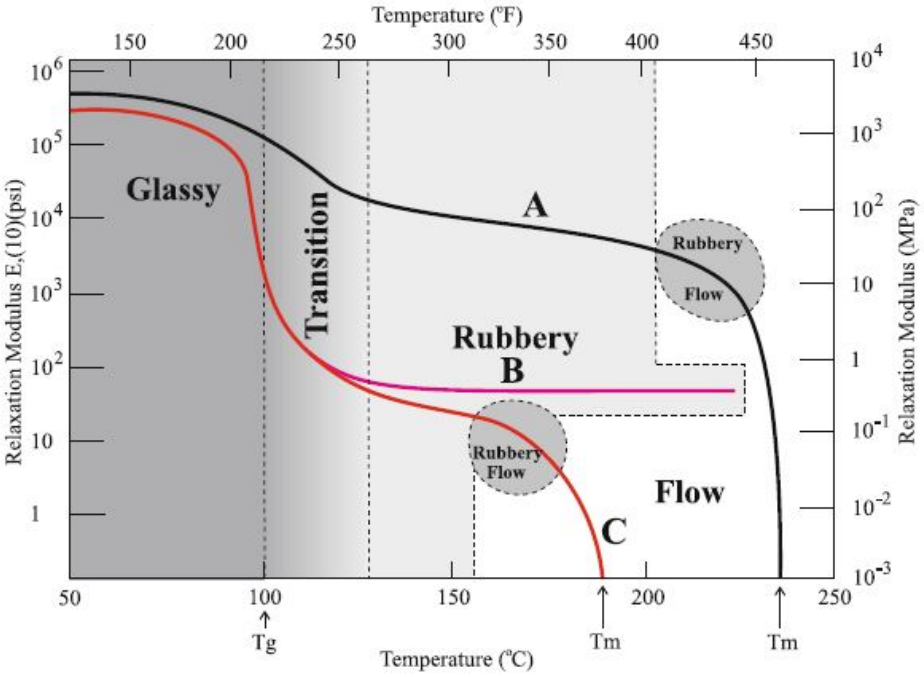


**Fig. 1.7:** The regions of state presented for a crystalline polystyrene (A), a lightly cross-linked one (B) and an amorphous one (C) [5].

### 1.1.4 Relative free volume

On basis of dilatometric measurements the glass transition temperature can also be defined by the relative free volume. The volume of a polymer can be differentiated in the volume of the chains and the one among the polymer chains [44]. The *occupied volume* $v_0$ represents the volume of the molecules and the one which is also associated with the vibrational motions. There are gaps and holes within the chains which can be considered as the *free volume* $v_f$. The occupied and the free volume change linearly over temperature whereby the slope of the free volume changes at the glass transition temperature. The figure 1.8 shows a schematic example of the relative volume in dependence on the temperature for a semi-crystalline polymer and an amorphous one. The uniform change of the occupied volume can be traced back to an increase of vibrational motion of the molecules over a rising temperature [44]. This discontinuity of the free volume is caused by a sudden expansion of the free volume above the glass transition temperature. In the theory of *Cohen and Turnbull* [12] the free volume is assumed to be random distributed in the polymer and at the glass transition temperature an additional free volume is brought in during the change of regions. It can be redistributed without a change in energy. For a more detailed explanation see e.g. [12]. Such discontinuities can also be found for the heat capacity and for the compressibility [16].

The coefficient of thermal expansion can be consulted in conjunction with the *fractional free volume* due to the poorly defined relative volume. The fractional free volume $f$ is the ratio between the free one and the relative one. Above the glass transition temperature the fractional free volume is assumed to change linearly [44].

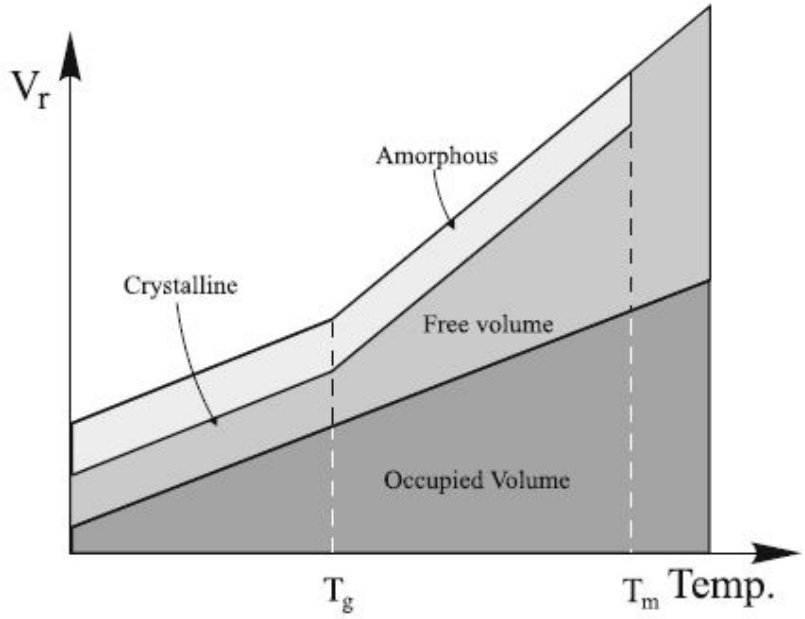


**Fig. 1.8:** The dependence of the relative volume over temperature for a semi-crystalline polymer and an amorphous one. The relative volume consists of the free one and the occupied one whereas the change of free volume is discontinuous [5].

## 1.2 Composites

The term *composite* referring to materials indicates a combination of two or more different materials on a macroscopic scale which only yields to a useable material as a compound. They basically consist of a *matrix* which has to be reinforced and the *reinforcement* itself [23]. The aim of a composite is to achieve higher and better properties than their individual components which can be improved stiffness, strength, fatigue life or lower weight. In general composite materials have been existing in nature for millions of years. Natural occurring composites are for example wood, bones or bamboo. The first documented synthetic composite in humankind are mud bricks reinforced with straw which were used to build huts by the Israelites. In the ancient Egypt wood was cut and rearranged to achieve higher strength, a lower thermal expansion and smaller swelling due to lesser water absorption. In the Medieval for example armour and weapons were forged and set together by the use of different materials [23]. Today synthetic composites have a wide area of application for example in the building, aviation or naval industry [11].

### 1.2.1 Structure of composites

#### 1.2.1.1 Matrix

The main part of a composite is the matrix which is supposed to distribute the load on the tougher reinforcement but the role of a matrix is way more complex in the composite. Two important tasks of a matrix are to maintain the desired position of the reinforcement and provide adhesiveness among the individual components. In general the thermo-mechanical stability, shear, compressive, transverse strength and durability of the composite is mostly determined by the matrix itself. As already mentioned the loads are distributed over the matrix on the reinforcement material but it also protects them from the environment and wearout [3]. The material of the matrix can be different but the tasks remain the same in the composite.

The matrix material is chosen in dependence of the maximum use temperature. Some of those materials are displayed in figure 1.9 over their maximum use temperature. The arrow represents the direction for materials with low density and a higher use temperature which are considered as *advanced materials* [3]. Those advanced materials can be certain polymers like polyimides, metals like aluminium, ceramics like silicon carbide and carbon.

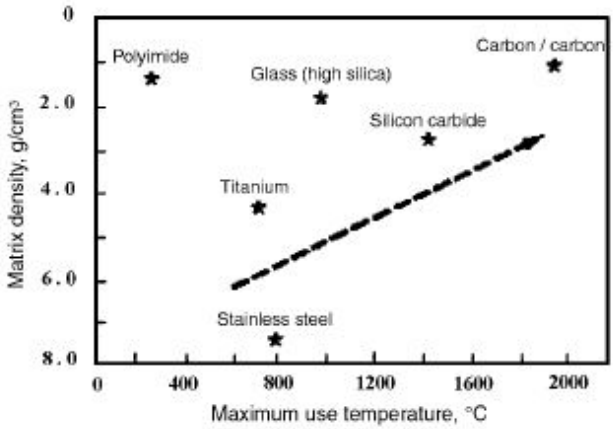


**Fig. 1.9:** Maximum use temperature of different matrix materials sorted by their density. The arrow points in the direction of materials with low density and higher use temperatures [3].

#### 1.2.1.2 Reinforcement

The second main part of a composite is the reinforcement material which only receives its final shape in the compound. In general its tasks are to reinforce, improve or compensate the downsides of the matrix in respect to stiffness, strength or sensibility to cracks. For improving the strength or stiffness the reinforcement material has to satisfy the condition of a higher modulus than the pure matrix. The reinforcement is considered to carry the main part of the load [3].

The reinforcements can occur in different shapes and in diverse materials. In general the application determines their shape and also their material which underlies the restriction of chemical compatibility with the matrix [3]. They mostly occur as continuous and short fibres and as particles. Those are presented as examples in the figures 1.10 to 1.12. Some well known fibre materials are carbon, glass and aramide but they can also consist of polyethylene, polyamide or basalt [46]. A possibility to characterize continuous, short fibres and particulates reinforcements is the *aspect ratio* [3], defined as

$$a = \frac{l_\mathrm{r}}{d_\mathrm{r}} \tag{1.1}$$

where $l_\mathrm{r}$ is the length and $d_\mathrm{r}$ the diameter of the reinforcement. When the aspect ratio is infinite, greater, equal or smaller than one the reinforcement is a continuous fibre, short fibre, sphere and platelet, respectively.

**Fig. 1.10:** Continuous glassfibres assembled to rovings and spooled on a bobbin [46]

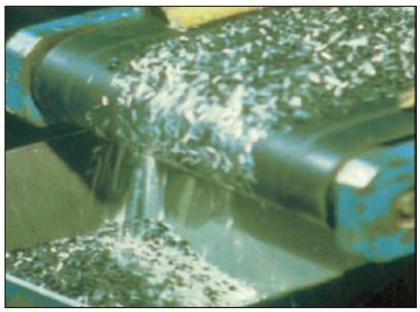

**Fig. 1.11:** Chopped glassfibres transported on a conveyor belt [46]

**Fig. 1.12:** Microballoons Q-21 from *HP-Textiles* https://www.bacuplast.de/hilfsmittel/fuellstoffe.html last viewed on 9 December 2019

### 1.2.2 Classification of composites

A classification of composites can be done in a number of ways. Hull et.al. [22] roughly distinguishes composites by their appearance between natural, micro- and macro-composites at which those classes especially the micro-composites are partitioned into more detailed subclasses. The most common natural composites are bones and wood. For a micro-composite Hull et.al. takes metallic alloys, reinforced thermoplastics or sheet moulding compounds as examples and for a macro-composite helicopter blades or reinforced concrete beams as an example. The micro-composites are subclassified in the microscopic appearance of the reinforcement in the matrix [22] which are

- Continuous fibres
- Short fibres
- Particulates

- Dispersion strengthened
- Lamellar structures
- Skeletal networks
- Multicomponent

The reinforcement type can depend on the matrix material and their assignment of the reinforcement to a specific matrix is not meaningful due to the wide area of applications. For example short fibres can be used in polymers but also used in ceramics.

It is also possible to classify composites only by their matrix materials. Chung et.al. [11] classifies composites into five classes of materials whereas Choo et.al. [10] only divides them into four. According to [11] those classes are

- Polymer-matrix
- Cement-matrix
- Metal-matrix
- Ceramic-matrix
- Carbon-matrix

where the classes except the cement-matrix are sorted by temperature in ascending order. In lightweight design polymer-matrix composites are inevitable and used in e.g. aircraft, sporting goods and also for vibrational damping applications. Cement-matrix composites can occur in different forms depending on their support media e.g. in structural buildings, steel-reinforced concrete or grout. Metal-matrix composites are often considered to be only alloys but they can also appear as a compound which are commonly used for e.g. indexable tips or drill bits. For higher temperature applications, e.g. engine, air- or spacecraft components, ceramic-matrix composites or in absence of oxygen carbon-matrix composites can be used [11]. Some of the mentioned matrix types are displayed as an example in the figures from 1.13 to 1.16.

**Fig. 1.13:** Carbon fibre reinforced epoxy bicycle frame [30]

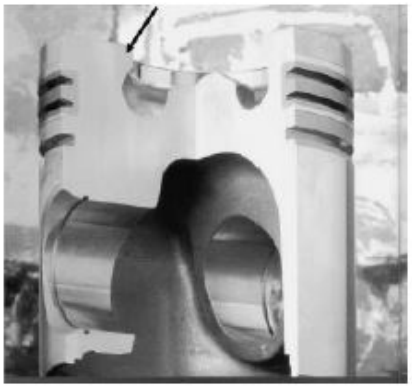

**Fig. 1.14:** Aluminium piston with fibre reinforced combustion bowl [24]

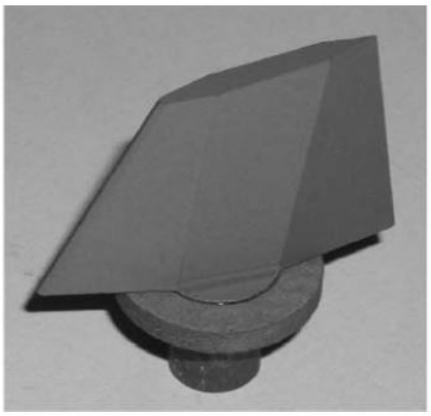

**Fig. 1.15:** Jet vane consisting of carbon fibre reinforced silicon carbide [28]

**Fig. 1.16:** Carbon-carbon brake disks [25]

### 1.2.3 Properties

The material properties of composite materials can differ a lot from conventional engineering materials and their characteristics can be modifications of traditional materials or completely new ones which requires new methods. Conventional engineering materials are often *homogeneous* and *isotropic* which means that the material properties are independent of the position and also independent of the orientation at a point in the body respectively. Composites on the other hand are *inhomogeneous* materials and their material behaviour is dependent of the reinforcement orientation which can be *anisotropic* or *orthotropic*. Fully anisotropic materials have completely different material properties at a point in the body for all directions and there are no symmetry planes existing in terms of properties. For orthotropic materials their properties only differ in three perpendicular directions at a

point in a body and also there are three perpendicular planes of symmetry in terms of properties [23].

In general the properties of reinforced composites depend on many microstructural factors. Those are the mechanical properties of the individual components, aspect ratio, volume fraction and reinforcement orientation. The influence of those factors have a different impact on the composite properties. For an effective processing, manufacturing and performance of composites those factors and their effects have to be characterized [22].

#### 1.2.3.1 Rule of mixture

The *rule of mixture* is the simplest analytical method to characterize mechanical properties in and transverse to the fibre direction of continuous fibre reinforced composites. The rules of mixture is based on strain and stress coupling of fibre and matrix in and transverse to the fibre direction respectively [22].

The volume of a composite consists of the ones from the matrix, fibre and voids. It is assumed that the composite is perfectly manufactured and the void volume is negligibly small against the others. Then the composite volume only consists of the fibre volume and the matrix volume. The ratios between the partial volumes and the composite's volume are the volume fractions of the fibre and of the matrix [26], expressed as

$$\frac{V_\mathrm{f}}{V_\mathrm{c}} + \frac{V_\mathrm{m}}{V_\mathrm{c}} = v_\mathrm{f} + v_\mathrm{m} = 1 \tag{1.2}$$

where $V_\mathrm{f}$, $V_\mathrm{m}$ and $V_\mathrm{c}$ are the volumes of the fibre, matrix and the composite respectively. The volume fractions of fibre and matrix are denoted as $v_\mathrm{f}$ and $v_\mathrm{m}$ respectively. The fibre volume fraction is practically limited due to the maximum packaging density of the fibres and for a further explanation it is referred to e.g. [38].

When a force is applied in fibre direction and assuming strain coupling the rule of mixture for the Young's modulus in fibre direction is obtained, as

$$E_{\mathrm{c},1} = v_\mathrm{f} \cdot E_\mathrm{f} + (1 - v_\mathrm{f}) \cdot E_\mathrm{m} \tag{1.3}$$

where $E_\mathrm{f}$ and $E_\mathrm{m}$ are the Young's moduli of the fibre and the matrix in fibre direction respectively.

When a force is applied transverse to the fibre direction and assuming stress coupling the inverse rule of mixture for the Young's moduli transverse to the fibre direction is obtained, as

$$E_{\mathrm{c},2} = \frac{E_\mathrm{f} \cdot E_\mathrm{m}}{(1 - v_\mathrm{f}) \cdot E_\mathrm{f} + v_\mathrm{f} \cdot E_\mathrm{m}} \tag{1.4}$$

where $E_{c,2}$ is the Young's modulus transverse to the fibre direction but the predictions are to low. A more detailed derivation of both equations is displayed in e.g. [26].

#### 1.2.3.2 Effect of fibre volume fraction on elastic mechanical properties

Both equations of the rule of mixture can be used to demonstrate the influence of the fibre volume fraction on the mechanical properties. The figure 1.17 shows the dependency of the Young's moduli on the fibre volume fraction. The blue and the orange curve represent the moduli in and transverse the fibre direction respectively. The modulus $E_{c,1}$ changes linearly over the fibre volume fraction. The transverse modulus $E_{c,2}$ increases slowly with rising volume fraction and at high fibre volume fractions it changes rapidly.

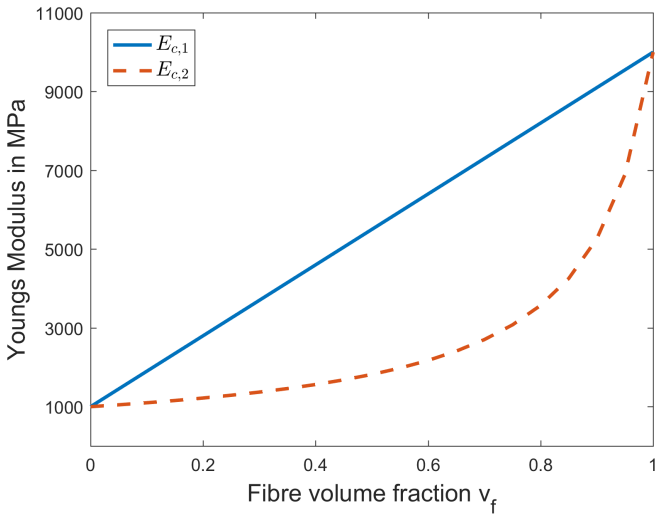


**Fig. 1.17:** The Young's moduli in (blue) and transverse (orange) to the fibre direction plotted against the fibre volume fraction by using the rule of mixture for the chosen moduli $E_f = 10000$MPa and $E_m = 1000$MPa.

## 1.3 Problem statement and Aim of work

A uni-directional reinforced composite consisting of elastic fibres and a linear viscoelastic matrix leads to a linear viscoelastic composite which is dominated by the matrix in terms of viscoelasticity and time-temperature behaviour [20]. Replacing the elastic fibres with linear viscoelastic ones results in non-trivial overall viscoelastic properties and time-temperature behaviour of the composite. This thesis focuses on the effective relaxation behaviour and the time-temperature behaviour of a composite with two different viscoelastic materials. The research will use the periodic microfield approach, a common micromechanical modelling strategy, implemented as a unit cell in a finite elements software which is subjected to different load cases. To achieve the effective relaxation behaviour and the time-temperature behaviour the data evaluation is released to MATLAB.

The aim of this work is to collect information about the relaxation and time-temperature behaviour of a composite with two viscoelastic constituents used as a thin ply. The gained knowledge may be used later for an implementation as a shell element with direction dependent time-temperature-shift functions in a finite element software.

## 1.4 Literature overview on viscoelastic composites

A test procedure is presented in [47] to determine the time-temperature response for a unidirectional reinforced composite which consists of elastic graphite fibres and a viscoelastic epoxy matrix. Those creep tests include strip tension specimens which are loaded in different angles to the fibre direction and at various temperatures. The effective behaviour of the composite in fibre direction is elastic for all temperatures whereas the effective behaviour transverse to the fibre direction varies by temperature.

In [7] the time-temperature behaviours of multi-phase composites are investigated by using the dynamic correspondence principle in the frequency domain. The composite consists of a matrix and cylindrical inclusions whereby both phases are individually viscoelastic and thermorheologically simple. It is assumed that the inclusion remains stiffer at all times than the matrix. The different time-temperature behaviours of the composite's constituents cause a thermorheologically complex behaviour of the composite and the effective moduli has a different character for each temperature.

In [6] the effective properties of a viscoelastic composite with multiple viscoelastic phases are determined numerically. A finite element model is used to obtain the composites effective properties by applying the dynamic correspondence principle of viscoelasticity. The results show a dominance of the matrix relating to the composites properties but for

higher frequencies the loss modulus is dominated by the phase which has a larger loss modulus.

In [8] different micromechanic methods are compared which are used to determine the effective properties for uni-directional composites with only viscoelastic phases. Both phases are ideally viscoelastic systems which have different instantaneous moduli, long-term ones and different relaxation times. The Mori-Tanaka method is extended for viscoelastic materials and the finite element unit cell method is implemented for a squared and a hexagonal fibre arrangement. The predictions of the squared and hexagonal arrangement and the prediction of the Mori-Tanka method are close to each other whereby the squared arrangements leads to a slighter stiffer behaviour. The Mori-Tanaka method is a faster implemented method for predictions but it is only accurate enough for moderate fibre volume fractions and it does not provide any further information about stress contours in comparison to the unit cells.

For the sake of completeness in [34] a micromechanical model is presented which is extended for a uni-directional non-linear thermo-viscoelastic composite. A unit cell is used to obtain the effective material properties whereby the accuracy of the prediction is improved by the use of tangent stiffness matrices of fibre and matrix. The results of the simulation are compared with those of an experiment.

The effective relaxation behaviour of a composite with two viscoelastic components is expected to be similarly assembled like in the case for pure elastic constituents. In fibre direction the relaxation is mainly dominated by the fibre and matrix dominated in the transverse direction. The relaxation for a shear load is also expected to be dominated by the matrix. According to the results of [7] the time-temperature behaviour is expected to be thermorheologically complex with different characters over temperature.

# Chapter 2

# Theoretical principals

## 2.1 Linear elasticity

Every solid body deforms under a constant load, and when it is able to completely retain its original shape after the load has been removed, the solid body is called *elastic*. Forces and moments cause stresses in the solid and this stress state is described by six stress components at one infinitesimal small volume of the body [17]. These stress components can be expressed in tensorial form or by using the Voigt notation as a vector. For a plane stress condition the six components are reduced to three and can now be written as

$$\underline{\sigma} = \begin{bmatrix} \sigma_{11} & \sigma_{22} & \sigma_{12} \end{bmatrix}^{\mathrm{T}} \tag{2.1}$$

where $\sigma_{ii}$ is a normal stress and $\sigma_{ij}$ is the in-plane shear stress.

The deformations can be divided into a relative movement within the body and a rigid body motion where the latter is uniform throughout the solid. The relative movement and the displacements are related by *kinematic* equations [17] and can be written in linear form as

$$\varepsilon_{kl} = \frac{1}{2}\left(\frac{\partial u_k}{\partial x_l} + \frac{\partial u_l}{\partial x_k}\right) \tag{2.2}$$

where $u_k$ and $u_l$ are the displacements in the directions $k$ and $l$ respectively and $x_k$ and $x_l$ denote the $k$- and $l$-direction of the coordinate system.

This leads to six strain components which can also be similarly expressed as the stresses in the plane stress state by the Voigt notation as

$$\underline{\varepsilon} = \begin{bmatrix} \varepsilon_{11} & \varepsilon_{22} & \gamma_{12} \end{bmatrix}^{\mathrm{T}} \tag{2.3}$$

where $\varepsilon_{kk}$ is a normal strain and $\gamma_{kl} = 2\varepsilon_{kl}$ is the in-plane shear angle.

The stresses and strains are connected together by a material law. The simplest material law is a linear connection between stresses and strains, the so called *Hook's law* [17], which reads for plane stress condition,

$$\begin{bmatrix} \sigma_{11} \\ \sigma_{22} \\ \tau_{12} \end{bmatrix} = \begin{bmatrix} E_{1111} & E_{1122} & 0 \\ E_{2211} & E_{2222} & 0 \\ 0 & 0 & E_{1212} \end{bmatrix} \begin{bmatrix} \varepsilon_{11} \\ \varepsilon_{22} \\ \gamma_{12} \end{bmatrix} \tag{2.4}$$

The symmetric tensor which is containing the material parameters $E_{ijkl}$ is called *elasticity tensor* and is here given in Voig notation.

## 2.2 Viscoelasticity

Viscoelastic materials can be seen as a mixture between an elastic solid body and a liquid. In the simplest mechanical model the elastic and viscous part can be interpreted and visualized by a linear elastic spring and a dashpot respectively. The viscous behaviour of fluids can be easily visualized by a moving plate on a semi-infinite fluid which is displayed in figure 2.1.

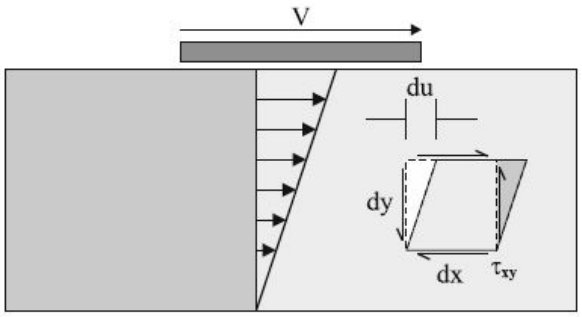


**Fig. 2.1:** Moving solid plate on a Newtonian fluid and the resulting shear deformation considering no slip boundary conditions [5]

When a solid plate is moved on the surface of a Newtonian fluid, a shear deformation in the fluid occurs which changes linearly from the bottom to the top considering no slip boundary conditions between plate, fluid and the fluid container [5]. This relationship is written as,

$$\tau = \mu \frac{d}{dt}\left(\frac{du}{dx_1}\right) = \mu \frac{d\gamma}{dt} \tag{2.5}$$

where $\mu$ is the fluid's viscosity, $\frac{du}{dx_1}$ is the velocity $V$ of the plate and $\frac{d\gamma}{dt}$ is the shear rate.

In general the viscoelasticity of polymers is way more complex and can be traced back to the micro-scale, the polymer chains. A viscoelastic polymer changes its material parameters over time or frequency due to the mobility of the chains and therefore it is reasonable to describe this behaviour in the time or frequency domain.

### 2.2.1 Rouse theory

The origin of the viscoelastic material behaviour can be derived from the polymer chains themself. The structure of the chains is described in several different theories and one of them is the theory of *Rouse* [39] or the *beads-spring* model [42].

In the Rouse theory a polymer chain gets substituted by a chain consisting of alternating beads and springs. The beads are seen as by fluid dragged spheres and they also contain the sub-chains. The springs are considered as Gaussian springs, see e.g. [42]. The figure 2.2 shows the described bead-spring chain of the Rouse theory. When a sphere moves through the fluid and the neighboured molecules a force occurs. In the theory of Rouse those forces are replaced by a continuum with viscosity. A main problem of this theory is the consistent treatment of polymer entanglements and their influence on the viscosity [42]. The Rouse and other theories are explained in a more detailed way in e.g. [18] or [9].

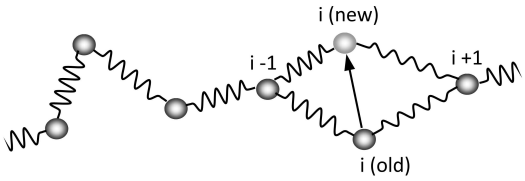


**Fig. 2.2:** Substituted polymer chain with beads and springs where bead $i$ moves from an old to a new position in the fluid - Source: http://polymerdatabase.com/polymer physics/BeadSpring.html last viewed on November 11, 2019

### 2.2.2 Viscoelastic phenomenons

The polymer chain movement and the resulting viscoelastic phenomenons can be either observed in transient experiments or in dynamic ones. The most common transient experiments are the relaxation and creep test at which a specimen is subjected to a constant strain or stress either as tension or shear load.

A typical dynamic experiment is subjecting the specimen to a harmonic varying strain which leads to the damping phenomenon [2].

#### 2.2.2.1 Creep

The viscoelastic phenomenon creep is an increasing deformation over time under a constant stress state. The stress is described by a magnitude and the Heaviside step function for a one-dimensional load case [29] in equation (2.6) as

$$\sigma(t) = \sigma_0 \mathcal{H}(t) \tag{2.6}$$

where $\sigma_0$ is the stress magnitude, $t$ the time and $\mathcal{H}(t)$ the step function which is defined as

$$\mathcal{H}(t) = \begin{cases} 0 & , \text{if } t < 0 \\ \frac{1}{2} & , \text{if } t = 0 \\ 1 & , \text{if } t > 0 \end{cases} \tag{2.7}$$

The Heaviside step function is an ideal application of the load and it assumes that the load is applied instantaneously. At the beginning the strain responds to the stress input with an initial strain, which can be considered as an instantaneous elastic behaviour of the material. Over time it increases continuously until an equilibrium state is reached [29]. When the load is removed, the strain drops and the residual strain converges to zero in the linear viscoelasticity. The figure 2.3 shows the explained creep and also the recovery phenomenon.

The ratio between the time-dependent strain and the constant stress is called *creep compliance* and for linear viscoelastic materials it is dependent on time but independent of the stress level. The creep compliance is expressed as

$$J(t) = \frac{\varepsilon(t)}{\sigma_0} \tag{2.8}$$

where $t$ is the time and $\sigma_0$ the applied constant stress.

At $t = 0$ the creep compliance is called *instantaneous* creep compliance and at the equilibrium state for $t \to \infty$ it is called *long-term* creep compliance. The instantaneous and long-term creep compliance are denoted with zero and the infinity symbol in the index respectively.

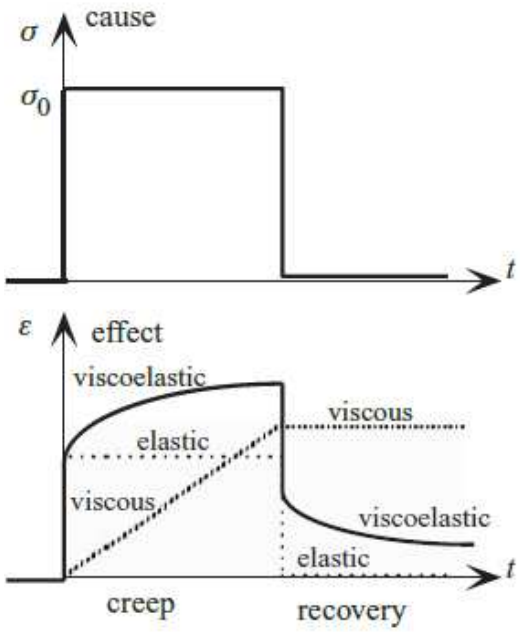


**Fig. 2.3:** Constant stress is applied as a step function which causes an instantaneous strain at $t = 0$ and strain increases over time until an equilibrium state is reached. When the stress is removed recovery takes place and the residual strain converges to zero for a linear viscoelastic material. [29]

#### 2.2.2.2 Relaxation

The relaxation phenomenon is a decreasing stress over time under a constant strain. For the one-dimensional deformation state the strain is defined in equation (2.9) by a magnitude and the already mentioned Heaviside step function,

$$\varepsilon(t) = \varepsilon_0 \mathcal{H}(t) \tag{2.9}$$

where $t$ is the time, $\varepsilon_0$ the strain magnitude and $\mathcal{H}(t)$ the Heaviside step function.

The applied strain causes an instantaneous stress, which also can be seen as an instantaneous elastic behaviour of the material. The stress decreases over time until it reaches an equilibrium [29]. When the constant strain is removed, recovery starts where the stress drops below zero and the residual stress converges to zero in the linear viscoelasticity. The relaxation phenomenon is displayed in figure 2.4.

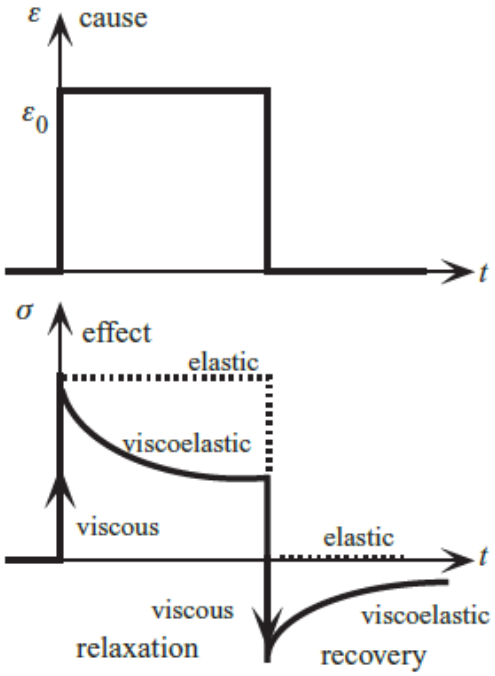


**Fig. 2.4:** Constant strain leads in the beginning to an instantaneous stress which decreases over time until an equilibrium state is reached. When the strain is removed the recovery takes place and the residual stress converges to zero for a linear viscoelastic material. [29]

The ratio between the time-dependent stress and the constant strain is called *relaxation modulus*. For linear viscoelastic materials the relaxation modulus is only dependent on time [29]. The relaxation modulus is expressed as,

$$E(t) = \frac{\sigma(t)}{\varepsilon_0} \tag{2.10}$$

where $t$ is the time, $E(t)$ the relaxation modulus and $\varepsilon_0$ the applied constant strain.

Similar to the creep compliance, for $t = 0$ the relaxation modulus is called *instantaneous* relaxation modulus and for $t \to \infty$ it is called *long-term* relaxation modulus.

#### 2.2.2.3 Damping

A one dimensional harmonic varying strain can be expressed by a magnitude, a sine function and its circular frequency. For a linearly viscoelastic material the figure 2.5 shows the stress-strain plot over time under a sinusoidal load, where the stress drags behind the strain. This drag can be considered as a damping behaviour of the material [29].

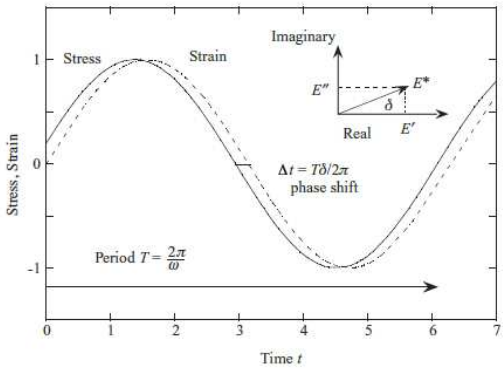


**Fig. 2.5:** Sinusoidal stress input and strain response over time - phase shift due to damping of viscoelastic material [29]

A more convenient method is to describe the phase lag between stress and strain as a complex number. Under consideration of the *Euler*'s equation the harmonic varying stress and the resulting strain can be described by the equations (2.11) and (2.12) respectively

$$\sigma(t) = \sigma_0 e^{i\omega t} \tag{2.11}$$

$$\varepsilon(t) = \varepsilon_0 e^{i(\omega t - \delta)} \tag{2.12}$$

where $\sigma_0$ and $\varepsilon_0$ are the magnitudes of stress and strain respectively, $t$ the time, $\omega$ the circular frequency and $\delta$ the *loss angle* which describes the mentioned drag between stress and strain.

The ratio between the harmonic varying stress and strain is called *dynamic stiffness*. The complex modulus consists of a real part, the *storage modulus*, and of an imaginary part, the *loss modulus*. The storage modulus and the loss modulus are components of the stress-strain ratio in and 90 degrees out of phase respectively [16]. The loss angle, the storage modulus and the loss modulus are dependent on the circular frequency. In equation (2.13) and (2.14) the complex modulus and the loss angle are expressed respectively,

$$\frac{\sigma(t)}{\varepsilon(t)} = E^* = E' + iE'' \tag{2.13}$$

$$\tan(\delta) = \frac{E''}{E'} \tag{2.14}$$

where $E^*$ is the complex modulus, $E'$ the storage modulus, $E''$ the loss modulus and $\delta$ the loss angle.

### 2.2.3 Constitutive law

For a viscoelastic material the material parameters are time-dependent and therefore the stress components can be obtained by integrating the product of material parameter and strain rate over time [36]. The stress-strain relation reads then in tensorial form

$$\sigma_{ij}(t) = \int_0^t R_{ijkl}(t-s)\dot{\varepsilon}_{kl}(s)ds \tag{2.15}$$

where $t$ is the time, $\sigma_{ij}(t)$ the stress component, $R_{ijkl}(t)$ the material parameter and $\dot{\varepsilon}_{kl}$ the strain rate.

For an orthotropic material under a plane stress condition the material parameters can be written as

$$\underset{\sim}{\mathbf{R}} = \begin{bmatrix} R_{1111}(t) & R_{1122}(t) & 0 \\ R_{2211}(t) & R_{2222}(t) & 0 \\ 0 & 0 & R_{1212}(t) \end{bmatrix} \quad \text{where} \quad R_{1122}(t) = R_{2211}(t) \tag{2.16}$$

where the entries $R_{ijkl}(t)$ are individually defined as relaxations functions which are expressed as a Prony-series expansion

$$R_{ijkl}(t) = R_{ijkl,0}\left[1 - \sum_q r_{ijkl,q}(1 - exp(-t/\tau^{r_{ijkl,q}}))\right] \quad \text{(no sum on ijkl)} \tag{2.17}$$

where $R_{ijkl,0}$ are the instantaneous values of the material tensor, $q$ is the number of Prony terms, $r_{ijkl,q}$ are the relative relaxation elements and $\tau^{r_{ijkl,q}}$ are the corresponding characteristic times [21].

## 2.3 Time-temperature dependency

The viscoelastic behaviour of polymers can be derived by molecule movements of the polymer chains. For example under a one-dimensional tensile stress the polymer gets initially stretched and over time the molecule chains try to align in direction of the tensile load [39]. These alignments cause an additional elongation over time and are referred to the creep phenomenon. For the movement of the polymer chains an activation energy is required which determines the time period. When the activation energy is low the polymer chains align themself in a shorter period of time and for a higher activation energy the alignment happens at longer time periods. Temperatures affect these times by either shortening or lengthening them at higher or lower temperatures respectively. This is called *time-temperature correspondence* [2].

Beside this relation there is also one between time and pressure which is called *time-pressure correspondence*. Both relations act independent from each other on the relaxation and retardation process [43].

### 2.3.1 Shifting factor

The influence of the temperature on the relaxation time can be derived from the *Rouse* equation. This equation describes the connection between the relaxation time of the $p^{\text{th}}$ segment of a molecule, the molecular weight of this chain segment $p$, the solution density, the viscosity of the dilute solution, the universal gas constant and the temperature [5]. A rearranged form of the *Rouse* equation is displayed with a constant right hand side, as

$$\frac{\tau_p \rho T}{\eta} = \frac{6M}{\pi^2 p^2 R} = \text{const.} \tag{2.18}$$

where $\tau_p$ is the relaxation time of the $p^{\text{th}}$ segment, $M$ the molecular weight of segment $p$, $p$ the number of segments per molecule, $\rho$ the solution density, $\eta$ the solution viscosity, $R$ the universal gas constant and $T$ the temperature.

The ratio between the relaxation times for an arbitrary temperature and a reference temperature results in the *shifting factor*. The shifting factor is obtained by the use of equation (2.18) and is expressed as

$$a_T = \frac{\tau_p(T)}{\tau_p(T_0)} = \frac{\eta}{\eta_0}\left(\frac{\rho_0 T_0}{\rho T}\right) \tag{2.19}$$

where $T$ is the arbitrary temperature and $T_0$ the reference temperature.

The shifting factor now allows to obtain the relaxation time at temperature $T$ only by knowing the relaxation time at a specific temperature. If all relaxation times are affected by temperature in the same way, the polymer is called *thermorheologically simple* [5]. Some polymers, especially polymer blends or co-polymers, do not satisfy the definition of thermorheologically simple and are instead called *thermorheologically complex*.

It is also possible to use the shifting principle for thermorheologically complex materials but this leads to misleading master curves and incorrect results. Therefore the shifting factor is considered to be additionally depend on the strain rate.

$$a_T = a_T(T, t) \tag{2.20}$$

In general for thermorheologically simple materials the shifting factors can either be found experimentally or by numeric equations.

### 2.3.2 Principle of reduced time

Beside the relaxation times it is also possible to use the shifting principle to obtain various material parameters at different temperatures. Therefore the material behaviour is researched over time at a constant temperature and over temperature at constant time. The long-term behaviour of the polymer can be obtained by the time-temperature correspondence principle. In this principle the relaxation at temperature $T_1$ can be expressed by the relaxation at temperature $T_2$ in a shorter time assuming $T_1 < T_2$ [39]. The mathematical form is displayed as

$$E(t, T_1) = E(t_{\text{red}}, T_2) \text{ where } t_{\text{red}} = \frac{t}{a_{\text{T}}} \text{ , } T_1 < T_2 \tag{2.21}$$

where $E(t, T_i)$ is the relaxation modulus at temperature $T_i$ and $t_{\text{red}}$ is the *reduced time*. The reduced time can be linked by the shifting factor to the original time $t$ and a schematic representation of equation (2.21) is displayed in figure 2.6 for the compliance $J(t)$.

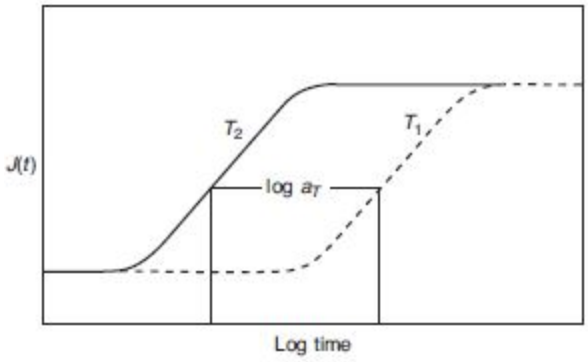


**Fig. 2.6:** Presenting the principle of reduced time for the compliance over a logarithmic time scale for the temperatures $T_1$ and $T_2$ where $T_1 < T_2$. The increase of the compliance starts earlier at the higher temperature $T_2$ than for temperature $T_1$ [44].

### 2.3.3 Williams-Landel-Ferry equation

The Williams-Landel-Ferry (WLF) equation is a numeric equation to obtain the shifting factor for various polymers [16]. It is assumed that the relaxation and retardation behaviour of polymers arises from the micro-Brownian or segmental movement of the polymer chains which is derived by considering the theory of fractional free volume [43].

The starting basis of the WLF-equation is the empirical *Doolittle* equation which describes the dependency of the viscosity of liquids on the free volume [43]. When this

equation is used and expressed in terms of shifting factor the equation (2.22) is obtained, expressed as

$$\log a_{\mathrm{T}} = \frac{B}{2.303}\left(\frac{1}{f} - \frac{1}{f_0}\right) + \log\frac{T_0\rho_0}{T\rho} \tag{2.22}$$

where $f_0$ is the fractional free volume at the reference temperature $T_0$, $f$ the ratio of the specific volumes, $B$ an arbitrary constant, $T$ the temperature, $\rho$ and $\rho_0$ the density at temperature $T$ and $T_0$ respectively. The second term on the right hand side of this equation is often neglected due to the small change of the specific volume and therefore the constant $B$ may differ very slightly [16]. The fractional free volume is assumed to change linearly with temperature and is expressed as

$$f = f_0 + \alpha_f(T - T_0) \tag{2.23}$$

where $\alpha$ is the rate of change of the free volume. The equations (2.22) and (2.23) are used to obtain the equation (2.24) which is also known as the WLF equation. It is applicable for temperatures above the glass transition temperature.

$$\log a_{\mathrm{T}} = -\frac{(B/2.303f_0)(T - T_0)}{f_0/\alpha_f + T - T_0} = -\frac{C_1(T - T_0)}{C_2 + T - T_0} \tag{2.24}$$

The constants $C_1$ and $C_2$ can be empirically determined at an arbitrary reference temperature $T_0$. The data for a large number of polymers are fitted by the WLF-equation and the average constants $C_1$ and $C_2$ are 17.44 and 51.6 respectively. Ferry remarked for those "universal" constants they should be seen as last resort in absence of any specific data [16].

According to [16] the WLF-parameters depend on the chosen reference temperature and it is possible to convert those parameters from the reference temperature to an arbitrary one. The conversion relation is defined as,

$$C_1' = \frac{C_1C_2}{C_2 - T - T_0} \tag{2.25}$$

$$C_2' = C_2 + T - T_0 \tag{2.26}$$

where $C_1'$ and $C_2'$ are the WLF-parameters for an arbitrary temperature $T$.

### 2.3.4 Arrhenius equation

A popular way to describe a material parameter like the viscosity in dependence of temperature is by the use of an activation energy. An example for the viscosity is displayed as

$$\eta(T) = A \exp\left(\frac{\mathcal{E}}{\mathcal{R}\mathcal{T}}\right) \tag{2.27}$$

where $\eta(T)$ is the temperature dependent viscosity, $A$ a pre factor, $\mathcal{E}$ the activation energy, $\mathcal{R}$ the universal gas constant and $T$ the temperature.

The shifting factor can also be defined by the ratio between the viscosity at temperature $T$ and $T_0$. This leads to the *Arrhenius* equation which is a well-established numerical method to determine the shifting factor by an activation energy. It is expressed as

$$\log a_{\mathrm{T}} = \frac{\mathcal{E}}{\mathcal{R}}\left(\frac{1}{T} - \frac{1}{T_0}\right) \tag{2.28}$$

where $\mathcal{E}$ is the activation energy, $\mathcal{R}$ the universal gas constant, $T$ the temperature and $T_0$ the reference temperature according to [27]. The activation energy describes the needed energy at which the polymer chains are able to move against each other. The Arrhenius equation is also applicable for temperatures much higher than the glass transition temperature [9]. The Arrhenius and the WLF-shifting equations are equal for small temperature regions and can be converted in both ways.

## 2.4 Introduction into micromechanics

A composite structure can be viewed and examined on different length scales which can be the macro, meso- and microscale at which the macro- and the microscale are used for two basic approaches. In the macromechanical approach the composite is considered to be a statistically homogenized and anisotropic structure at the global scale which ignores the arrangement of constituents [1]. For the characterization of the correlation between the mechanical behaviour of the composite and those of its individual components can be analysed only at the microscale. At the microscale the composite is viewed as a heterogeneous material at which the arrangement of constituents is considered under the restriction of a regular arrangement. Beside the interaction between the matrix and fibre the microscale also allows to predict the overall material behaviour and the failure behaviour of the composite [1]. For the sake of completeness, the mesoscales are length scales in between the micro- and macroscale. Those intermediate length scales are used at the lamina level of layered composites and the arbitrary numbers of mesoscales in between

have to be differently chosen for each research case. Some examples of the mentioned length scales are displayed in figure 2.7.

The microstructure of many inhomogeneous materials is often statistically homogeneous and volume averaged properties are defined for such systems at which the properties are independent of the size and location of the volume element under the restriction that it is a sufficiently large one. When the volume element contains all necessary information about the description of the microstructure it is called *reference volume element* [4]. The stresses and strains are considered to vary "slowly" at the macro- and "fast" at the microscale. The slow variations are not evident in absence of macroscopic gradients whereas the fast fluctuations of local stresses and strains are induced by the inhomogeneities. Those fast fluctuations can be averaged over the volume which leads to the macroscopic properties and is known as *homogenization*. The other way round is known as *localisation* at which the loads of the larger scale are transferred to a lower one [4].

There are three well established modelling strategies for a resolved microstructure of a composite which are the *periodic microfield approach*, *embedded configuration* and *windowing approach* [4]. A fully resolved configuration and all mentioned strategies are schematically displayed in figure 2.8.

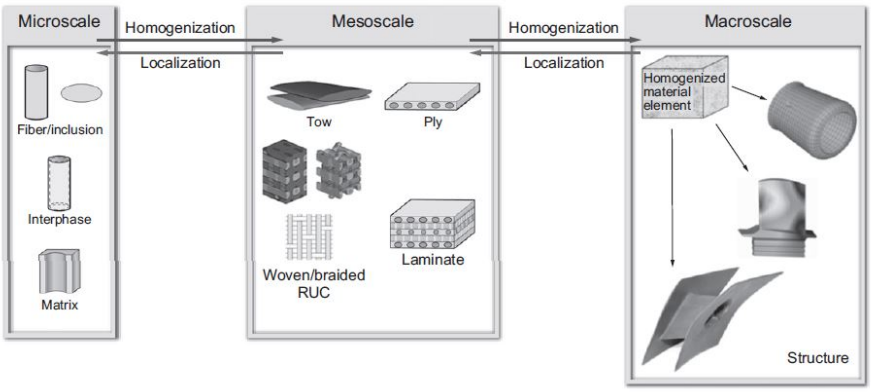


**Fig. 2.7:** Illustration of the length scales for analysing a composite at which the length scales can be switched by homogenization and localization [1].

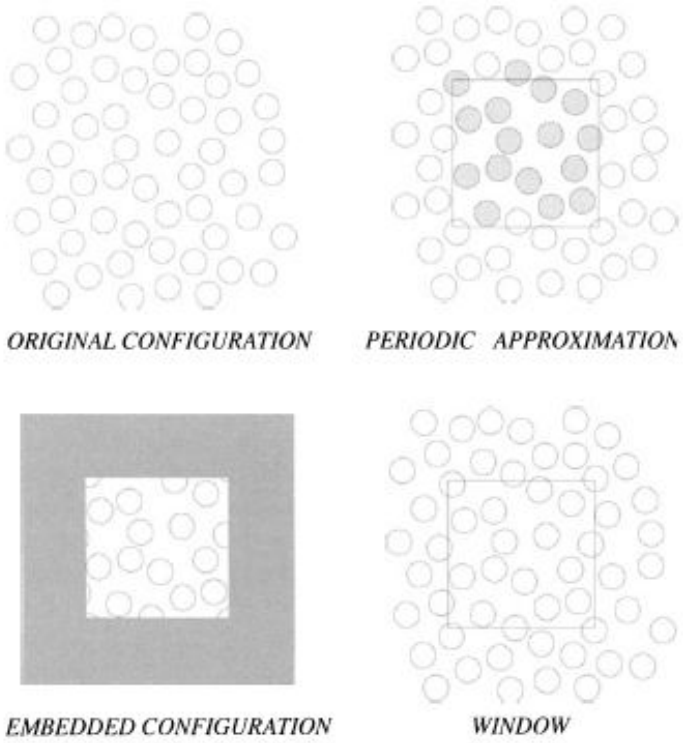


**Fig. 2.8:** Schematic configuration of inhomogeneities included within a matrix and the different microgeometries for the modelling strategies periodic microfield, embedded cell and windowing approach [4].

## 2.5 Periodic microfield approach

The periodic microfield approach is a numerical method which is used to determine the behaviour of an infinite material with periodic phase arrangement under a mechanical far field load or uniform temperature fields. This method basically aims to approximate microstructured materials and uses a periodically repeating unit cell to describe the microgeometry which allows to observe the strain and stress fields. Those fields are separated into a constant macroscopic part and the periodically varying fluctuations which can be resolved by a microscopic coordinate for resolving local characteristics of the unit cell [4]. The equation (2.29) shows an example of the separated strain field,

$$\varepsilon(z) = \langle\varepsilon\rangle + \varepsilon'(z) \tag{2.29}$$

where $\langle\varepsilon\rangle$ denotes the constant macroscopic strain, $\varepsilon'(z)$ the periodically varying strain fluctuations and $z$ is the microscopic coordinate. A set of periodicity vectors is used to describe the periodic phase arrangement whereby the spatial dimension of the problem defines the amount of the periodicity vectors $\mathbf{p}_n$ [40]. In general the arrangement of fibres

in the matrix of such repeating unit cells can have different forms which are displayed in figure 2.9.

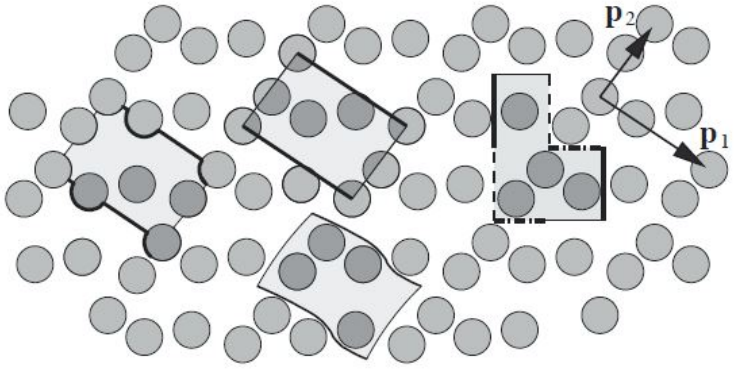


**Fig. 2.9:** Some examples of possible shapes of unit cells which can be found in a two-dimensional periodic arrangements of inhomogeneities. The periodicity vectors $\mathbf{p}_1$ and $\mathbf{p}_2$ describe the directions of periodic arrangement. The different line styles represent opposite faces of some arranged cells [40].

### 2.5.1 Boundary conditions

A periodic arrangement of the unit cells with their prescribed boundary conditions has to result in valid tilings of the undeformed state but also in the deformed one in which gaps and overlapping of neighboured cells are not allowed. Unphysical constraints on their deformations are also not allowed to occur. The boundary conditions are determined by appropriate deformation modes for all load cases which are studied. In the periodic microfield analysis the major boundary types are *periodic*, *symmetric* and *anti-symmetric* boundary conditions. Despite the numerical method which is used to solve the problem, one or a combination of these three types has to be used on any exterior boundary of the unit cell [4].

A perfect match of neighboured cells in the undeformed state as well as in the deformed one can be achieved by choosing reference faces and nodes which are used to describe the deformation of the other faces and nodes of the unit cell. The reference faces and nodes are then called master faces and master nodes whereas the other ones are assigned with the tag slave [40]. A two-dimensional squared unit cell is consulted to explain the different boundary types and compass directions are used to denote the nodes and also the side faces of the unit cell. The periodic type of the boundary conditions is the most general and versatile type which is capable of handling any possible deformation of the unit cell. For this boundary type the periodically varying microscopic displacements of the

North-East slave node and North and East slave faces can be expressed by the North-West and South-East master nodes and South and West master faces. These relations are displayed in the left part of figure 2.10 and expressed as

$$\mathbf{u}_{\mathrm{N}}(z_1) = \mathbf{u}_{\mathrm{S}}(z_1) + \mathbf{u}_{\mathrm{NW}} \qquad \mathbf{u}_{\mathrm{E}}(z_2) = \mathbf{u}_{\mathrm{W}}(z_2) + \mathbf{u}_{\mathrm{SE}} \qquad \mathbf{u}_{\mathrm{NE}} = \mathbf{u}_{\mathrm{NW}} + \mathbf{u}_{\mathrm{SE}} \tag{2.30}$$

where $z_1$ and $z_2$ are the microscopic coordinates, $\mathbf{u}_{\mathrm{N}}(z_1)$, $\mathbf{u}_{\mathrm{S}}(z_1)$, $\mathbf{u}_{\mathrm{E}}(z_2)$ and $\mathbf{u}_{\mathrm{W}}(z_2)$ are the displacements of the North, South, East and West faces respectively and $\mathbf{u}_{\mathrm{NW}}$ and $\mathbf{u}_{\mathrm{SE}}$ are the North-West and South-East nodes respectively [40]. When the symmetry plane of the phase arrangement and faces of rectangular or hexahedral unit cells coincide for the undeformed state as well as for the deformed state, the periodic boundary conditions can be simplified to the symmetric ones. These boundary conditions are displayed in middle of figure 2.10 and are expressed as

$$u_{\mathrm{E}}(z_2) = u_{\mathrm{SE}} \qquad v_{\mathrm{N}}(z_1) = v_{\mathrm{NW}} \qquad u_{\mathrm{W}}(z_2) = 0 \qquad v_{\mathrm{S}}(z_1) = 0 \tag{2.31}$$

where the components of the displacement vectors are denoted as $u$ and $v$ [40]. The counterpart of the symmetric boundary conditions are the anti-symmetric ones or point-symmetry ones. Those require pivot points or centres of symmetry at least on one face of the unit cell which causes further restrictions in terms of permitted microgeometries and load cases. An example of a unit cell with anti-symmetric boundary conditions is displayed on the right side of figure 2.10 and can be expressed as

$$\mathbf{u}_{\mathrm{U}}(s) + \mathbf{u}_{\mathrm{L}}(s) = 2\mathbf{u}_{\mathrm{P}} \qquad v_{\mathrm{N}}(z_1) = v_{\mathrm{NW}} = 2v_P \qquad v_{\mathrm{S}}(z_1) = 0 \qquad u_{\mathrm{W}}(z_2) = 0 \tag{2.32}$$

where $\mathbf{u}_{\mathrm{P}}$ is the deformation vector of the pivot point, $s$ is a local coordinate that is centred on the pivot point and $\mathbf{u}_{\mathrm{U}}(s)$ and $\mathbf{u}_{\mathrm{L}}(s)$ denote the deformation vectors of pairs of points $U$ and $L$ [40].

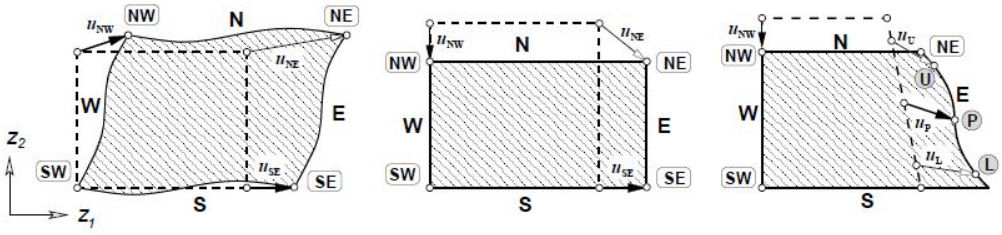


**Fig. 2.10:** Two-dimensional squared unit cells with periodic (left), symmetric (middle) and anit-symmetric (right) boundary conditions. The corner nodes and side faces are denoted with compass directions whereby the South-West node and West and South face are used as master node and faces respectively. [4].

### 2.5.2 Initiation of load

A unit cell with the appropriate boundary conditions is subjected to a far field load and returns the micromechanical behaviour. This linkage between the microscopic fields and the macroscopic ones is achieved by either the *asymptotic homogenization* or the *method of macroscopic degrees of freedom* [4].

The *asymptotic homogenization* is an elegant and mathematical method for linking micro- and macroscale. Two different sets of coordinates are introduced whereby one set describes the micro- and the other one the macroscale. The ratio between the macroscale coordinates and the ones of the microscale is a scaling parameter which describes the ratio between the characteristic lengths of the scales. It is used to expand displacements, strains and stresses and when those are introduced into strain-displacement relations, equilibrium equations and stress-strain relations, a set of differential equations are obtained. This boundary problem can be then solved numerically [4].

The *method of macroscopic degrees of freedom* uses nodal forces or displacements at master nodes for far field stresses or strains respectively. When a force is applied at a master node the corresponding slave nodes are also applied with an equivalent load. For strains the method of macroscopic degrees of freedom uses the homogeneous macroscopic strain and evaluates the specified displacements at master nodes [4].

# Chapter 3

# Methodology

## 3.1 Introduction

The viscoelastic behaviour of a composite and its development over time can be easily achieved by using a combination of an appropriate micromechanical modelling strategy and a finite element program. A suitable strategy is the periodic microfield approach to achieve the mechanical properties of the composite whereby those characteristics are determined for a plane stress state. The microstructure of a uni-directional composite is already discretizised and provided as a unit cell in a given input file. The used unit cell has got periodic boundary conditions and the global ones are used to define the load cases. It represents a uni-directional composite with a fibre volume fraction of 40% whereby the two constituents are viscoelastic materials and the corresponding time-temperature-shift functions are completely different from each other.

The finite element software *Abaqus 2018* [41] from *Dassault Systems* is used for the simulations of the viscoelastic behaviour of the unit cell. The simulation procedure is subdivided into two main steps, a *static* and a *visco* step whereby *Abaqus* uses only the instantaneous values in the static step and the changing material parameters at each time step in the visco step. Both steps are required for an approximation of the appropriate stress response for a Heaviside step function.

## 3.2 Coordinate system

A Cartesian coordinate system is introduced for describing the directions in the unit cell with its axes *1*, *2* and *3* and its origin is positioned at master node $M_0$. The fibre direction is characterised by the distance between the master nodes $M_0$ and $M_Z$ which will be superposed with the direction *1* of the coordinate system. The axis *2* will be congruent with the distance between the master nodes $M_0$ and $M_X$ which describes one of

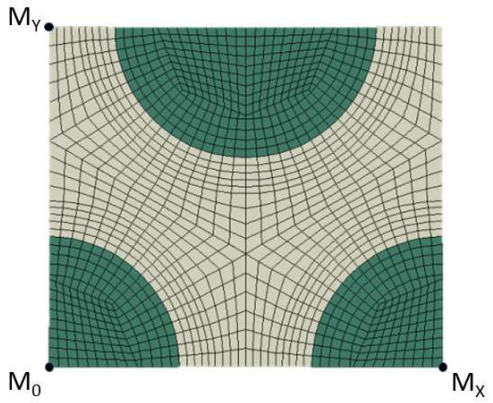


**Fig. 3.1:** Two coloured unit cell with visible master nodes at the edges- fibres and matrix are green and beige marked respectively

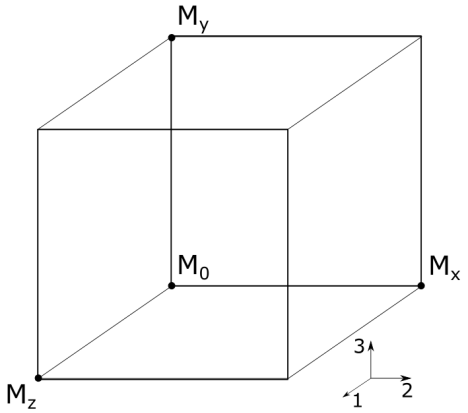


**Fig. 3.2:** Definition of the coordinate system

**Tab. 3.1:** Given unit cell dimensions

| | Distance | Length in $\mu$m |
|---|---|---|
| $l_1$ | $M_0$-$M_Z$ | 0.752391623 |
| $l_2$ | $M_0$-$M_X$ | 1.50478325 |
| $l_3$ | $M_0$-$M_Y$ | 1.30318052 |

the two directions transverse to the fibres. The other transverse direction is defined by the distance between the master nodes $M_0$ and $M_Y$ which is congruent with the axis *3* of the coordinate system. The figures 3.1 and 3.2 show the locations of the master nodes in the unit cell and the described definition of the coordinate system respectively.

The master nodes are used to define the directions of the coordinate system but they also describe the size of the unit cell. In table 3.1 the dimensions of the unit cell are listed.

## 3.3 Material parameters

Two different viscoelastic materials have to be chosen for the material input of the unit cell which are both individually considered to be isotropic and thermorheologically simple. The ratio between the Young's moduli of fibre and matrix should be greater than ten and the parameters of their shifting functions should also be different. Disregarding the chemical compatibility issues of material combination the interphase between fibre and matrix is supposed to be perfect.

**Tab. 3.2:** Parameters for fractional Zener model in the frequency domain including storage modulus $E_{f=0}$, the ratio $d$ between loss modulus and storage modulus, the reciprocal of frequency at maximal sotrage modulus $2\pi\tau$, order of fractional derivation and the loss angle $\delta_\infty$ for $f \to \infty$.

| Parameter | |
|---|---|
| $E_{f=0}$ | 10.36 GPa |
| $d$ | 5.251 |
| $2\pi\tau$ | 5.254 $\mu$s |
| $\kappa$ | 0.1595 |
| $\delta_\infty$ | 1.15° |

### 3.3.1 Fibre

The fibre material is chosen to be a polyamide PA6 whose material properties were obtained by a dynamic mechanical analysis and fitted by a fractional Zener model over a large frequency range during a project work [15], [35]. This numerical model is used to calculate the viscoelastic material data in the frequency domain at the reference temperature of 40°C.

The Fourier transformed fractional Zener model mathematically describes the complex modulus over the frequency expressed as

$$E^*(\mathrm{i}f) = E_{f=0} + E_{f=0}(d-1)\frac{(\mathrm{i}2\pi f\tau)^\kappa}{1+(\mathrm{i}2\pi f\tau)^\lambda} \text{ where } d = \frac{E_{f\to\infty}}{E_{f=0}} \tag{3.1}$$

where $f$ is the frequency, $E^*(\mathrm{i}f)$ the complex modulus, $E_{f=0}$ the storage modulus at frequency zero, $E_{f\to\infty}$ the storage modulus for $f \to \infty$, $2\pi\tau$ the reciprocal of frequency at maximal storage modulus, $\kappa$ and $\lambda$ are orders of fractional derivations [15]. The used values of the parameters are displayed in table 3.2 excepting the parameter $\lambda$ which is obtained by

$$\tan(\delta_\infty) = \tan(\frac{\pi}{2}(\kappa-\lambda)) \tag{3.2}$$

where $\delta_\infty$ is the loss angle for $f \to \infty$ [35]. The complex modulus is computed for a specific frequency range which steps are manually chosen to achieve a good fit for the Prony terms later with *Abaqus* and are listed in table 3.3.

The Poisson ratio of the fibre is assumed to stay constant over frequency and the transverse contraction is set at 0.39 which is a typical value for polyamides. The calculated

**Tab. 3.3:** Frequency steps in Hertz for the calculation of the complex modulus

| | | | | | | | | | |
|---|---|---|---|---|---|---|---|---|---|
| $5 \cdot 10^{-4}$ | $1 \cdot 10^{-3}$ | $5 \cdot 10^{-3}$ | $1 \cdot 10^{-2}$ | $5 \cdot 10^{-2}$ | $1 \cdot 10^{-1}$ | $5 \cdot 10^{-1}$ | $1 \cdot 10^{1}$ | $5 \cdot 10^{2}$ | $5 \cdot 10^{3}$ |
| $5 \cdot 10^{4}$ | $1 \cdot 10^{6}$ | $5 \cdot 10^{6}$ | $5 \cdot 10^{7}$ | $1 \cdot 10^{8}$ | $5 \cdot 10^{8}$ | $1 \cdot 10^{9}$ | $5 \cdot 10^{9}$ | $1 \cdot 10^{10}$ | $5 \cdot 10^{10}$ |

**Tab. 3.4:** Material parameters of the fibre in the time domain including the instantaneous moduli $E_{0,\mathrm{F}}$, long-term moduli $E_{\infty,\mathrm{F}}$, Poisson ratio $\nu_{\mathrm{F}}$, reference temperature $T_{\mathrm{Ref,F}}$ and the WLF-parameters $C_{1,\mathrm{F}}$ and $C_{2,\mathrm{F}}$.

| | |
|---|---|
| $E_{0,\mathrm{F}}$ | 54.4 GPa |
| $E_{\infty,\mathrm{F}}$ | 10.36 GPa |
| $\nu_{\mathrm{F}}$ | 0.39 |
| $T_{\mathrm{Ref,F}}$ | 313.15 K |
| $C_{1,\mathrm{F}}$ | 42.8 |
| $C_{2,\mathrm{F}}$ | 218.6 |

values of the complex modulus have to be converted for the input of the viscoelastic data and therefore it is referred to the *Abaqus* manual [41]. The parameters of the shifting parameters for Williams-Landel-Ferry equation were also determined in the mentioned project work [35] and are listed in table 3.4 where $E_{0,F}$ is the instantaneous modulus, $E_{\infty,\mathrm{F}}$ the long-term modulus, $\nu_{\mathrm{F}}$ the Poisson ratio, $T_{\mathrm{Ref,F}}$ the reference temperature and $C_{1,\mathrm{F}}$ and $C_{2,\mathrm{F}}$ are the WLF-parameters. The complete input data of the fibre for ABAQUS is listed in section A.1. The software automatically fits a Prony series and those values are presented together with the relaxation behaviour in chapter 4.

It is noted that the instantaneous and the long-term moduli of the fibre material are above common ones of conventional polymers. Those values are accordingly taken and thus it is referred to [35].

### 3.3.2 Matrix

The matrix material is a provided but unspecified polyester resin whereas only the elastic and viscoelastic properties are known which are determined at a temperature of 20°C. The corresponding parameters of the Arrhenius like time-temperature-shift function are also known. The material parameters of the matrix are listed in the table 3.5 in which $E_{0,\mathrm{M}}$ is the instantaneous modulus, $E_{\infty,\mathrm{M}}$ the long-term modulus, $\nu_{\mathrm{M}}$ Poisson ratio, $T_{\mathrm{Ref,M}}$ the reference temperature and $\mathcal{E}_{\mathrm{A,M}}$ the activation energy for the Arrhenius shift function. The complete input data for ABAQUS is listed in section A.2. The software also automatically

fits a Prony series for the matrix material input and those values are presented together with the relaxation behaviour in chapter 4.

**Tab. 3.5:** Material parameters of the matrix in the time domain including the instantaneous moduli $E_{0,\mathrm{M}}$, long-term moduli $E_{\infty,\mathrm{M}}$, Poisson ratio $\nu_{\mathrm{M}}$, the reference temperature $T_{\mathrm{Ref,M}}$ and the activation energy $\mathcal{E}_{\mathrm{A,M}}$.

| | |
|---|---|
| $E_{0,\mathrm{M}}$ | 1350 MPa |
| $E_{\infty,\mathrm{M}}$ | 700 MPa |
| $\nu_{\mathrm{M}}$ | 0.35 |
| $T_{\mathrm{Ref,M}}$ | 293.15 K |
| $\mathcal{E}_{\mathrm{A,M}}$ | 448 kJmol$^{-1}$ |

## 3.4 Loading cases and boundary conditions

The complete macroscopic relaxation behaviour is describable by a material tensor similar to the one of equation (2.16) whereas the entries itself are discrete values over time. By the use of the same mathematical structure of equation (2.4) the linear viscoelastic material law for a plane stress state is then expressed as,

$$\begin{bmatrix} \sigma_{11}(t) \\ \sigma_{22}(t) \\ \sigma_{12}(t) \end{bmatrix} = \begin{bmatrix} R_{1111}(t) & R_{1122}(t) & 0 \\ R_{2211}(t) & R_{2222}(t) & 0 \\ 0 & 0 & R_{1212}(t) \end{bmatrix} \begin{bmatrix} \varepsilon_{11}(t) \\ \varepsilon_{22}(t) \\ 2\varepsilon_{12}(t) \end{bmatrix} \tag{3.3}$$

where the time dependent strain components are defined by Heavyside step functions and are expressed as

$$\varepsilon_{kl}(t) = \varepsilon_{kl,0}\mathcal{H}(t) \tag{3.4}$$

One strain component has to be applied individually to determine the entries of the material tensor which results in a two axial stress response. In ABAQUS each node has three translational degrees of freedom which are in general manipulated by applying arbitrary displacements to achieve either strains or constraints when those are set to zero. The periodic microfield approach allows to apply a displacement at one single master node to achieve a uniform strain in the same direction. To achieve a plane stress state in the *1-2* plain of the unit cell and thus the validity of equation (3.3) some degrees of freedom have to be locked. This plain stress state is obtained when the transversal contraction in direction *3* is allowed and so the master node $\mathrm{M}_0$ has to be completely

locked whereas master node $M_Y$ is only restricted for the directions *1* and *2*. ABAQUS returns the reaction forces of the master nodes at the individual time steps which are then used to calculate the macroscopic stresses.

The tensor entries $R_{1122}$ and $R_{2211}$ are equal due to the symmetry of the material tensor and can be obtained either in the first or in second load case. Nevertheless those are determined in both load cases and are used for a check in terms of tensor symmetry.

### 3.4.1 Uniaxial strain in fibre direction

In the first load case only the strain component $\varepsilon_{11}$ is applied in the direction *1* which leads to a simplification of equation (3.3) to

$$\sigma_{11}(t) = R_{1111}(t)\,\varepsilon_{11} \tag{3.5}$$

$$\sigma_{22}(t) = R_{1122}(t)\,\varepsilon_{11} \tag{3.6}$$

$$\varepsilon_{22} = \varepsilon_{12} = 0 \tag{3.7}$$

where the material tensor entries $R_{1111}(t)$ and $R_{1122}(t)$ are obtained from. The displacement $l_1$ is applied at master node $M_Z$ in the direction *1* and its arbitrary magnitude is set at $0.1\mu m$. The master node $M_X$ is not allowed to move in any direction and therefore all of its degrees of freedom are locked. The remaining degrees of freedom of master node $M_Z$ can not be manipulated and stay unchanged.

### 3.4.2 Uniaxial strain transverse to the fibre direction

In the second load case only the strain component $\varepsilon_{22}$ is applied in the direction *2* whereby equation (3.3) simplifies to

$$\sigma_{11}(t) = R_{2211}(t)\,\varepsilon_{22} \tag{3.8}$$

$$\sigma_{22}(t) = R_{2222}(t)\,\varepsilon_{22} \tag{3.9}$$

$$\varepsilon_{11} = \varepsilon_{12} = 0 \tag{3.10}$$

and results in the material tensor entries $R_{2211}(t)$ and $R_{2222}(t)$. The displacement $l_2$ is applied at master node $M_X$ in the direction *2* and like in the first load case the arbitrary magnitude is set at $2.0\mu m$. The rest of the degree of freedoms of master node $M_X$ are locked. The transversal contraction in direction *1* is hindered by locking the corresponding degree of freedom of master node $M_Z$.

### 3.4.3 In-plane shear strain

In the third and last load case only the shear angle component $\gamma_{12} = 2\varepsilon_{12}$ is applied in the *1-2* plain where equation (3.3) changes to

$$\sigma_{12}(t) = R_{1212}(t)\ \gamma_{12} = R_{1212}(t)\ 2\varepsilon_{12} \tag{3.11}$$

$$\varepsilon_{11} = \varepsilon_{22} = 0 \tag{3.12}$$

and results in the material tensor entryy $R_{1212}(t)$. The displacement $l_2$ is applied at master node $\mathrm{M}_X$ in direction *1* and this leads to a shearing of the unit cell. The arbitrary magnitude of the displacement is set at $2.0\mu m$. The remaining degrees of freedom of master node $\mathrm{M}_X$ and the only accessible degree of freedom of master node $\mathrm{M}_Z$ are also locked.

## 3.5 Temperature

The relaxation behaviour of the composite and its constituents is dependent on the chosen temperature for the simulation. In general higher temperatures lead to faster relaxations and lower temperatures to slower ones. Both time-temperature-shift functions underlie a restriction in terms of the allowable temperatures but due to the circumstance of unknown glass transition temperatures for fibre and matrix material, the reference temperatures are used to narrow the temperature region. The temperature interval is subdivided into five temperatures which are displayed in table 3.6. It is mentioned that for the time-temperature-shift of the fibre it is recommended not to use temperatures far below 30°C according to [35] due to the accuracy of the WLF-shift.

**Tab. 3.6:** Temperatures in °C used for simulation

| | | | | |
|---|---|---|---|---|
| 20 | 25 | 30 | 35 | 40 |

## 3.6 Data evaluation

The software MATLAB R2016b [33] is used for the data evaluation. In general the code is used to read the simulation output files line by line and only the numerical data of the static and the viscoelastic steps are transferred to the program.

The data includes the nodal displacements, reaction forces and temperature at all four master nodes. For each time step the stresses in fibre direction and transverse to the fibre direction and the in-plane shear stress are calculated as

$$\sigma_{11}(t) = \frac{F_{1,\mathrm{M_Z}}(t)}{A_\mathrm{Z}} \tag{3.13}$$

$$\sigma_{22}(t) = \frac{F_{2,\mathrm{M_X}}(t)}{A_\mathrm{X}} \tag{3.14}$$

$$\sigma_{12}(t) = \frac{F_{3,\mathrm{M_X}}(t)}{A_\mathrm{X}} \tag{3.15}$$

where $F_{i,\mathrm{M}_j}$ is the reaction force in direction $i$ at master node $\mathrm{M}_j$ and $A_i$ is the cross section with direction $i$ as surface normal. The strains have to be calculated as

$$\varepsilon_{kl} = \frac{\Delta l_k}{l_l} \tag{3.16}$$

where $l_l$ is the length of the unit cell and $\Delta l_k$ is the predefined nodal displacement. The macroscopic stress components and strain components are used to determine the material tensor entries which are the ratios between the stress and strain components which are expressed as

$$R_{1111}(t) = \frac{\sigma_{11}(t)}{\varepsilon_{11}} \tag{3.17}$$

$$R_{2222}(t) = \frac{\sigma_{22}(t)}{\varepsilon_{22}} \tag{3.18}$$

$$R_{1122}(t) = \frac{\sigma_{11}(t)}{\varepsilon_{22}} = \frac{\sigma_{22}(t)}{\varepsilon_{11}} = R_{2211}(t) \tag{3.19}$$

$$R_{1212}(t) = \frac{\sigma_{12}(t)}{2\varepsilon_{12}} \tag{3.20}$$

where $R_{ijkl}$ are the in equation (2.16) mentioned material tensor entries. All calculated values are plotted over time.

## 3.7 Fitting for WLF- and Arrhenius parameters

The composites effective viscoelastic properties represent an orthotropic material and therefore its time-temperature shifts are also separated into a shift of individual $R_{ijkl}$-elements. A WLF- and an Arrhenius shift function are used for shifting those elements. The arbitrary reference temperatures are set at 30°C and at the reference temperatures of matrix and fibre. The last two ones are only used for a better comparison in terms of the dominant part in the TTS-behaviour. Similar to equation 2.21 each time step is divided by the shifting factor to achieve the reduced time step and is once again presented as

$$t_{i,\mathrm{red}} = \frac{t_i}{a_{\mathrm{T},i}} \tag{3.21}$$

where $t_i$ is the time step $i$ of the reference relaxation curve at the temperature $T_{\mathrm{ref}}$ and $a_{\mathrm{T},i}$ the shifting factor.

Firstly the WLF-shifting parameters are determined by trial and error for a reference temperature of 30°C. Those are obtained by shifting the relaxation curve at the reference temperature to the ones at 25, 35 and 40°C. Some shifting factors are then calculated with those parameters for temperatures between 20°C and 40°C. They are used to fit an Arrhenius shifting function and thus obtaining the equivalent activation energy at the same reference temperature. The same procedure is also applied to the reference temperatures at 20°C and 40°C but they are additionally checked with the conversion relation of the WLF-function. The used relations are presented in the equations (2.25) and (2.26). The shifting parameters at 20°C and 40°C are later compared to the ones of the pure matrix and fibre, respectively.

## 3.8 Shift quality

The difference between the time steps of the shifted relaxation curve and the ones of the original relaxation curve are used to determine a quality of the shifted curves whereas the relaxation tensor entries at both times have to be equal. The quality measure reads,

$$Q_i = \frac{t_{i,\mathrm{Shift}} - t_{i,\mathrm{o}}}{t_{i,\mathrm{o}}} \tag{3.22}$$

where $t_{i,\mathrm{Shift}}$ is the time step $i$ of the shifted curve and $t_{i,\mathrm{o}}$ the original time step $i$. Due to the uneven distribution of the individual time steps, the original relaxation tensor entries are used at the time steps $t_{i,\mathrm{o}}$ and interpolated between the time data points of the shifted curve to obtain the shifted time steps. The MATLAB function *interp1* is used for the

**Tab. 3.7:** Interval borders of the time steps which are used to calculate the quality measure

| T in °C | time interval in s |
|---|---|
| 25 | $[4 \cdot 10^{-7}\ 2 \cdot 10^{7}]$ |
| 30 | $[1 \cdot 10^{-8}\ 3 \cdot 10^{6}]$ |
| 35 | $[2 \cdot 10^{-9}\ 6 \cdot 10^{4}]$ |
| 40 | $[2 \cdot 10^{-10}\ 5 \cdot 10^{3}]$ |

spline interpolation in the logarithmic domain. MATLAB needs strictly de- or increasing data points for the interpolations and therefore the useable data points are limited for the calculation. Those limits are presented in table 3.7 as intervals. The quality measure is calculated for each time step within the interval and an acceptable shift is obtained when the quadratic mean of the quality measure $Q_i$ is on average below ten per cent. The minimum and maximum of the quality measure are also determined whereas those are defined as the lowest and highest values of $Q_i$ respectively. The average, minimum and maximum of those calculated values are determined by the pre-defined MATLAB functions *rms*, *min* and *max* respectively.

# Chapter 4

# Results and Discussion

In the following the material tensor will be called relaxation tensor and their entries are labelled with an $R$ and four numbers in their indices. Revisiting the meaning of these indices they denote the stress component caused by the applied strain in the first two and the strain component itself in the last two numbers. The entries $R_{iijj}$ and $R_{ijij}$ will be called coupling and shear entry, respectively.

## 4.1 Relaxation behaviour

The relaxation behaviours of the composite, pure matrix and pure fibre are fully depicted by their relaxation tensor entries. A condensed form of presentation is used for the relaxation entries of the pure matrix and fibre due to their isotropic material behaviour.

### 4.1.1 Pure matrix

The figures 4.1, 4.2 and 4.3 show the relaxation tensor entries $R_{1111}$, $R_{1122}$ and $R_{1212}$ plotted for the temperatures between 20°C and 40°C over a logarithmic time scale respectively. The bumpy and wavy curve development over time is caused due to the limited amount of fitted Prony terms. The complete set of the fitted Prony-terms are presented in table 4.1 for the shear and the bulk moduli whereas ABAQUS used nine terms to fit the shear modulus and ten terms to fit the bulk modulus. The relative shear moduli, relative bulk moduli and the corresponding characteristic times are denoted as $g_i$, $k_i$, $\tau^{g_i}$ and $\tau^{k_i}$, respectively. All instantaneous and long-term values of the relaxation tensor entries are listed in the table 4.2.

All relaxation curves of the $R_{ijkl}$-elements have a distinct flat spot between $1 \cdot 10^{-7}$s and 10s. This is caused by a bigger difference of the characteristic times of two consecutive Prony terms. A second flat spot occurs below the first one but it is less distinct and those can also be traced back to a temporal gap between the characteristic relaxation

times of two neighboured Prony terms. A temperature increase of 5°C from the reference temperature of 20°C leads to a curve shift to the left and thus to faster relaxation times. The shifts for 30°C, 35°C and 40°C are analogue to the one at 25°C which shifts the relaxation curves about two, three and four decades to the left, respectively. Little kinks are present in the figures of relaxation entries $R_{1122}$ and $R_{1212}$ at the bottom right part which may be caused by a bad shifted characteristic time of a Prony term.

**Tab. 4.1:** Listing of the nine relative shear moduli $g_i$, ten relative bulk moduli $k_i$ and their corresponding characteristic times $\tau^{g_i}$ and $\tau^{k_i}$ of the Prony terms for the shear and bulk moduli. They are fitted with a root-mean error of about 0.19 for the shear modulus and of about 0.16 for the bulk modulus. The reference temperature and the Arrhenius shifting parameter of the pure matrix are again presented.

| | | | |
|---|---|---|---|
| $g_1 = 1.2050 \cdot 10^{-1}$ | $\tau^{g_1} = 7.9773 \cdot 10^{-3}$ | $g_2 = 9.2767 \cdot 10^{-2}$ | $\tau^{g_2} = 3.8008 \cdot 10^{1}$ |
| $g_3 = 1.0377 \cdot 10^{-1}$ | $\tau^{g_3} = 3.6754 \cdot 10^{3}$ | $g_4 = 1.1888 \cdot 10^{-1}$ | $\tau^{g_4} = 7.1097 \cdot 10^{4}$ |
| $g_5 = 1.1828 \cdot 10^{-1}$ | $\tau^{g_5} = 1.0173 \cdot 10^{6}$ | $g_6 = 9.8119 \cdot 10^{-2}$ | $\tau^{g_6} = 1.1190 \cdot 10^{7}$ |
| $g_7 = 6.6882 \cdot 10^{-2}$ | $\tau^{g_7} = 1.8765 \cdot 10^{8}$ | $g_8 = 6.6882 \cdot 10^{-2}$ | $\tau^{g_8} = 1.9965 \cdot 10^{8}$ |
| | $g_9 = 6.6882 \cdot 10^{-2}$ | $\tau^{g_9} = 1.9965 \cdot 10^{8}$ | |
| $k_1 = 1.0799 \cdot 10^{-1}$ | $\tau^{k_1} = 5.7235 \cdot 10^{-3}$ | $k_2 = 9.4060 \cdot 10^{-2}$ | $\tau^{k_2} = 2.0797 \cdot 10^{1}$ |
| $k_3 = 9.2107 \cdot 10^{-2}$ | $\tau^{k_3} = 2.1521 \cdot 10^{3}$ | $k_4 = 9.2109 \cdot 10^{-2}$ | $\tau^{k_4} = 4.2433 \cdot 10^{4}$ |
| $k_5 = 8.9420 \cdot 10^{-2}$ | $\tau^{k_5} = 3.3865 \cdot 10^{5}$ | $k_6 = 8.6350 \cdot 10^{-2}$ | $\tau^{k_6} = 1.8940 \cdot 10^{6}$ |
| $k_7 = 7.2754 \cdot 10^{-2}$ | $\tau^{k_7} = 1.0300 \cdot 10^{8}$ | $k_8 = 7.2754 \cdot 10^{-2}$ | $\tau^{k_8} = 1.0335 \cdot 10^{8}$ |
| $k_9 = 7.2754 \cdot 10^{-2}$ | $\tau^{k_9} = 1.0335 \cdot 10^{8}$ | $k_{10} = 7.2754 \cdot 10^{-2}$ | $\tau^{k_{10}} = 1.0335 \cdot 10^{8}$ |
| | $T_{\text{Ref}} = 20°\text{C}$ | $\mathcal{E} = 448\ \text{kJmol}^{-1}$ | |

**Tab. 4.2:** Listing of the instantaneous and long-term relaxation tensor entries of the pure matrix

| | $R_{1111} = R_{2222}$ in MPa | $R_{1122} = R_{2211}$ in MPa | $R_{1212}$ in MPa |
|---|---|---|---|
| $t = 0$ | 5 425.9 | 1 899.5 | 1 763.2 |
| $t \to \infty$ | 3 039.3 | 611.6 | 661.5 |

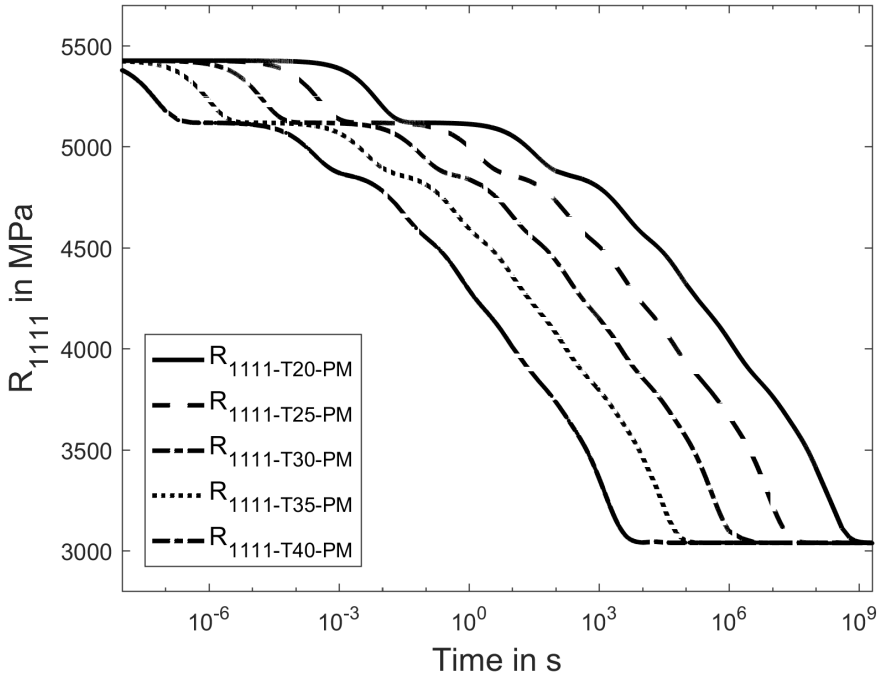


**Fig. 4.1:** Development of relaxation tensor entry $R_{1111}$ of pure matrix over logarithmic time scale at 20, 25, 30, 35 and 40°C

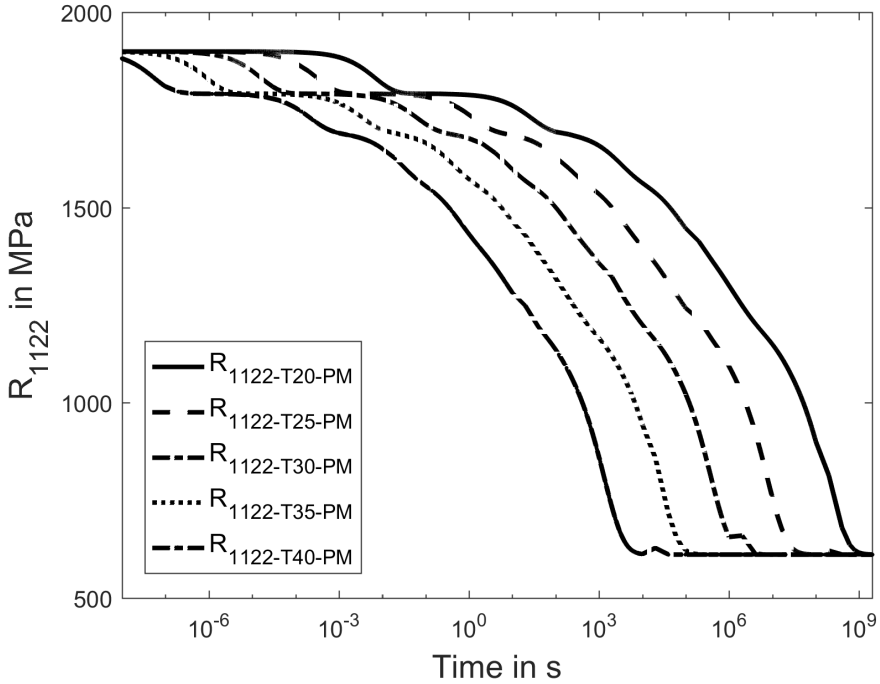


**Fig. 4.2:** Development of coupling tensor entry $R_{1122}$ of pure matrix over logarithmic time scale at 20, 25, 30, 35 and 40°C

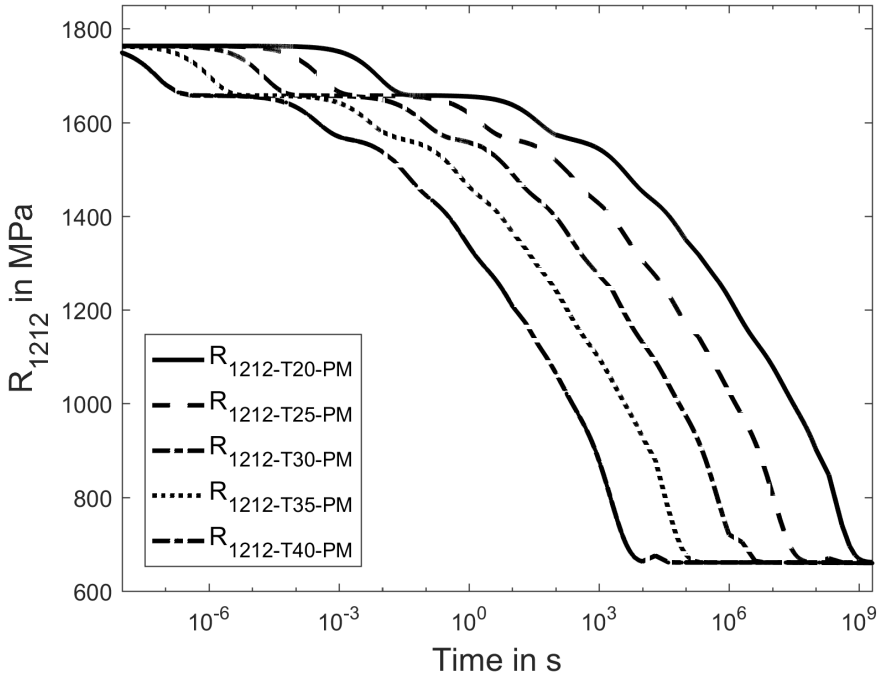


**Fig. 4.3:** Development of shear tensor entry $R_{1212}$ of pure matrix over logarithmic time scale at 20, 25, 30, 35 and 40°C

### 4.1.2 Pure fibre

The relaxation entries $R_{1111}$, $R_{1122}$ and $R_{1212}$ are presented in the figures 4.4, 4.5 and 4.6 for the pure fibre which are plotted over a logarithmic time scale for temperatures between 20 and 40°C. The bumpy and wavy curve development are also caused due to a limited amount of Prony terms. ABAQUS fits a set Prony-series for the fibre's shear and bulk moduli whereas both are identical due to the assumption of the constant Poisson's ratio. Therefore only the Prony-terms of the shear moduli are presented in the table 4.3. The relative shear moduli and their corresponding relaxations times are denoted as $g_i$ and $\tau^{g_i}$, respectively. The table 4.4 lists all instantaneous and long-term values of the relaxation tensor entries for the pure fibre.

Every relaxation curve has got a distinctive plateau in their development which is situated between 2s and $1 \cdot 10^7$s. This flat spot in the relaxation curve is also caused by a larger difference in terms of characteristic times of two consecutive Prony terms. The curve has also a visible "bend" in its development. A comparison of the Prony-terms and their corresponding characteristic relaxation times results in a temporal gap of two decades between the characteristic times of two neighboured Prony-terms. A temperature decrease of 5°C from the reference temperature of 40°C results in a curve shift of about one decade to the right side and thus the relaxation times are shifted to slower ones. The relaxation curves are shifted about two, three and four decades to the right for 30°C, 25°C and 20°C, respectively.

**Tab. 4.3:** Listing of the eight relative shear moduli $g_i$ their corresponding characteristic times $\tau^{g_i}$ for the shear moduli which are identical for the bulk modulus. They are fitted with a root-mean error of about 0.25. The reference temperature and WLF-shifting parameters of the pure fibre are again presented.

| | | | |
|---|---|---|---|
| $g_1 = 1.5998 \cdot 10^{-1}$ | $\tau^{g_1} = 2.3980 \cdot 10^{-10}$ | $g_2 = 1.5437 \cdot 10^{-1}$ | $\tau^{g_2} = 2.0653 \cdot 10^{-8}$ |
| $g_3 = 1.4565 \cdot 10^{-1}$ | $\tau^{g_3} = 1.1771 \cdot 10^{-6}$ | $g_4 = 1.1006 \cdot 10^{-1}$ | $\tau^{g_4} = 4.0447 \cdot 10^{-5}$ |
| $g_5 = 1.0862 \cdot 10^{-1}$ | $\tau^{g_5} = 2.1022 \cdot 10^{-3}$ | $g_6 = 7.3954 \cdot 10^{-2}$ | $\tau^{g_6} = 5.0652 \cdot 10^{-1}$ |
| $g_7 = 8.8166 \cdot 10^{-2}$ | $\tau^{g_7} = 3.3530 \cdot 10^{3}$ | $g_8 = 8.8166 \cdot 10^{-2}$ | $\tau^{g_8} = 5.1118 \cdot 10^{3}$ |
| $T_{\text{Ref}} = 40°\text{C}$ | $C_1 = 42.8$ | $C_2 = 218.6$ | |

**Tab. 4.4:** Listing of the instantaneous and long-term relaxation tensor entries of the pure fibre

| | $R_{1111} = R_{2222}$ in MPa | $R_{1122} = R_{2211}$ in MPa | $R_{1212}$ in MPa |
|---|---|---|---|
| $t = 0$ | 172 037.3 | 67 094.5 | 52 471.4 |
| $t \to \infty$ | 86 626.7 | 13 977.5 | 14 003.1 |

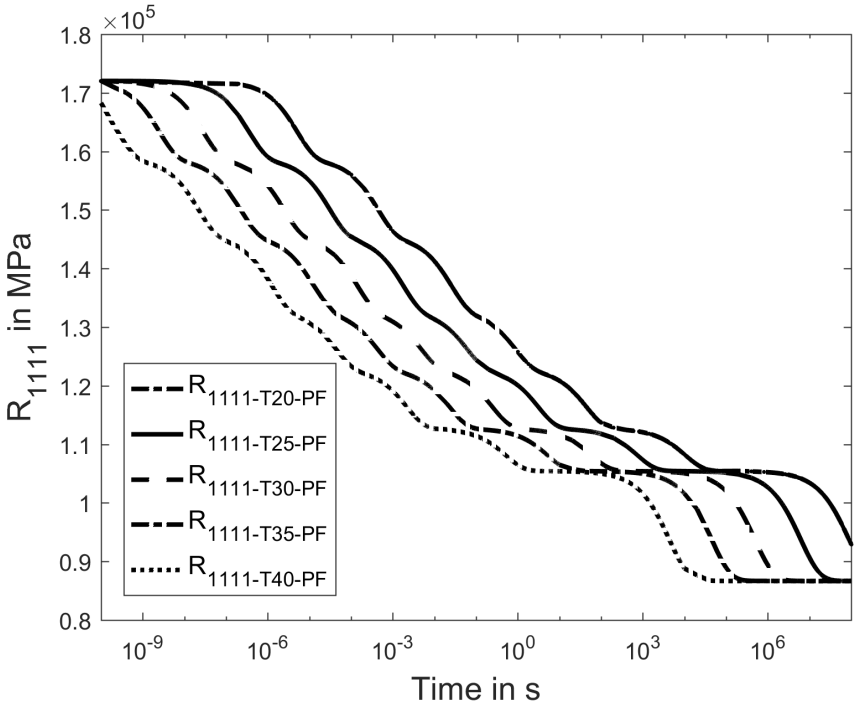


**Fig. 4.4:** Development of the relaxation tensor $R_{1111}$ of the pure fibre over logarithmic time scale at 20 ,25, 30, 35 and 40°C

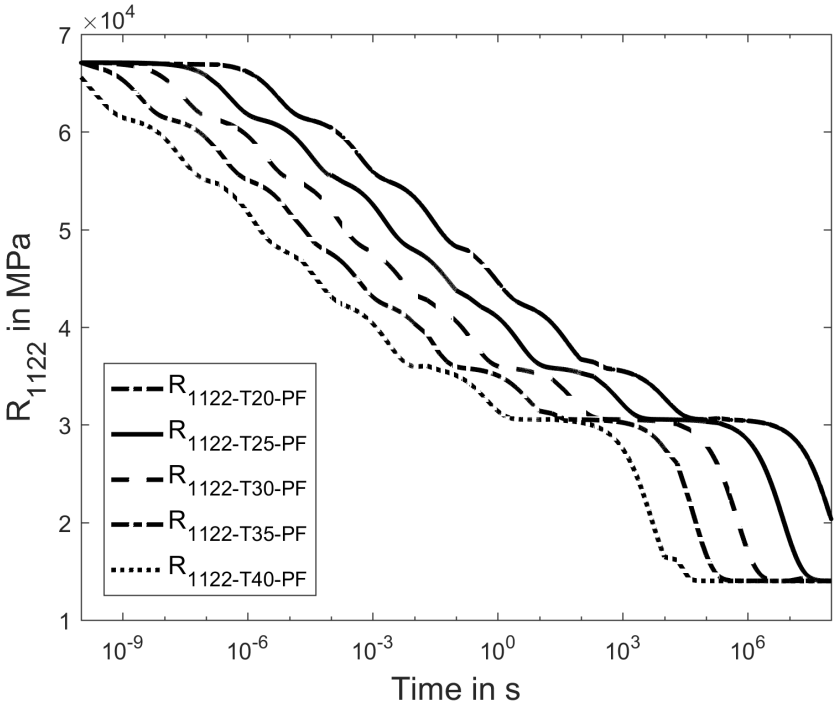


**Fig. 4.5:** Development of the coupling tensor $R_{1122}$ of the pure fibre over logarithmic time scale at 20, 25, 30, 35 and 40°C

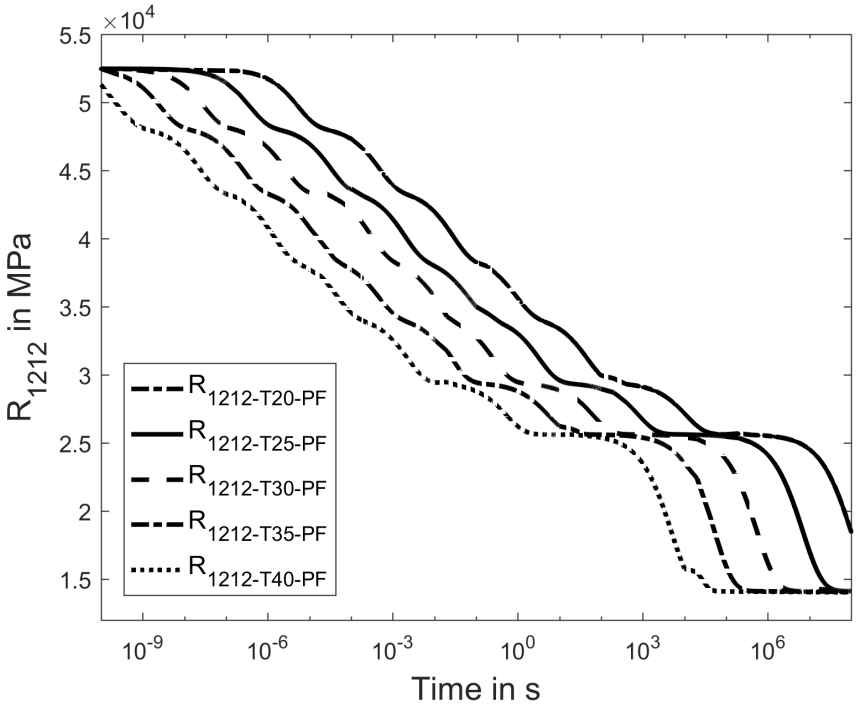


**Fig. 4.6:** Development of the shear tensor $R_{1212}$ of the pure fibre over logarithmic time scale at 20, 25, 30, 35 and 40°C

### 4.1.3 Composite

The figures 4.7, 4.8, 4.9 and 4.10 show the development of the relaxation tensor entries $R_{1111}$, $R_{2222}$, $R_{1122}$ and $R_{1212}$ over a logarithmic time scale respectively. The relaxation curves of the composite also result in bumpy and wavy ones due to the limited amount of Prony terms in the material input of fibre and matrix.

The relaxation tensor entry $R_{1111}$ has a similar development over time than the fibre. A distinctive similarity is the plateau region which also occurs in the relaxation development of the composite. At this spot the relaxation more slowly proceeds than in comparison to the pure fibre. The mentioned bend in the relaxation development of the pure fibre is also visible in the one of the composite. For all other relaxation tensor entries a distinctive flat spot occurs between about $2 \cdot 10^{-7}$s and 10s which is similar to the ones in the relaxation development of the matrix. Below this flat spot there is another less distinctive one that gets smaller with rising temperature. A temporal comparison of the relaxation times between composite, fibre and matrix further underpins the similarities and thus the influence of the fibre on the relaxation tensor entry $R_{1111}$ and of the matrix on the rest of the relaxation tensor entries.

**Tab. 4.5:** Listing of the instantaneous and long-term relaxation tensor entries of the composite

| | $R_{1111}$ in MPa | $R_{2222}$ in MPa | $R_{1122} = R_{2211}$ in MPa | $R_{1212}$ in MPa |
|---|---|---|---|---|
| $t = 0$ | 62 667.6 | 10 752.5 | 3 962.8 | 3 873.2 |
| $t \to \infty$ | 33 446.1 | 3 425.4 | 1 263.4 | 1 647.4 |

As expected, the composite has an mechanically orthotropical material behaviour with its distinct directions *1* and *2* according to the chosen coordinate system. A comparison between the shape of relaxation tensor entry $R_{1111}$ of the fibre and the one of the composite results in a clear dominance by the fibre. Both of them have a similar curve development and the conspicuous plateau of the fibre is also existing but it is less distinct due to the additional relaxation of the matrix. All other entries of the relaxation tensor are mainly dominated by the matrix which can also be derived from similar curve developments with respect to the matrix ones. For this material combination the composite has at first sight rather similar characteristics over different temperatures for each relaxation tensor entry and equal looking spacings in between. This can also be interpreted as a thermorheologically simple material behaviour. It cannot be stated yet whether the condition of thermorheological simplicity is satisfied or not.

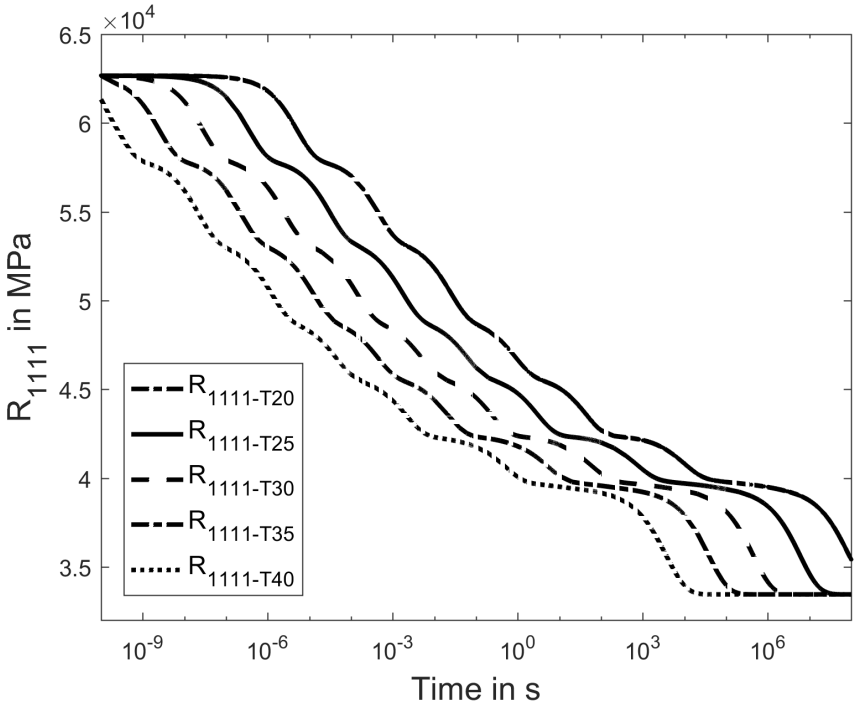


**Fig. 4.7:** Development of relaxation tensor entry $R_{1111}$ of the composite over a logarithmic time scale at 20, 25, 30, 35 and 40°C

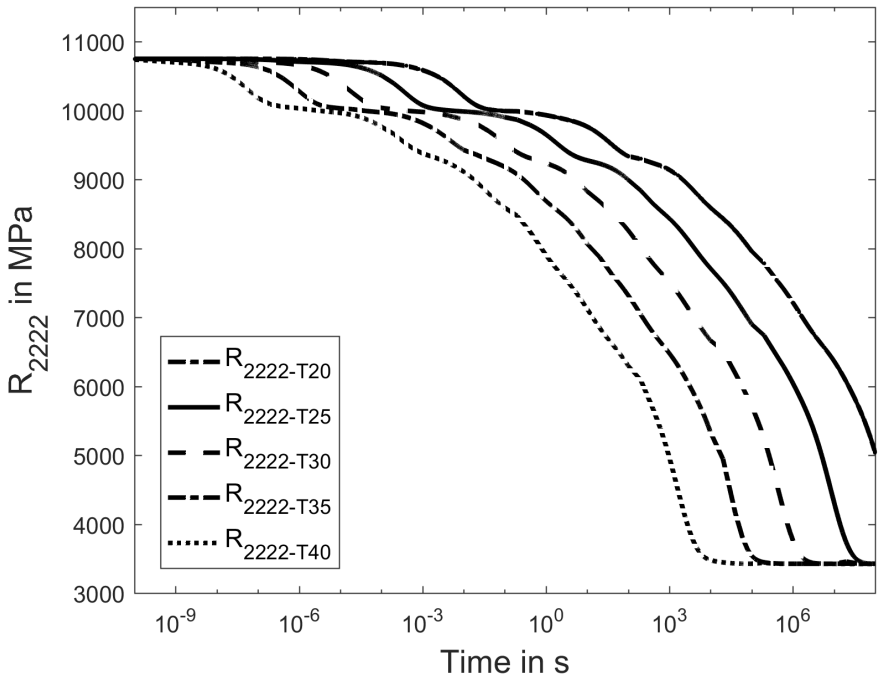


**Fig. 4.8:** Development of relaxation tensor entry $R_{2222}$ of the composite over a logarithmic time scale at 20, 25, 30, 35 and 40°C

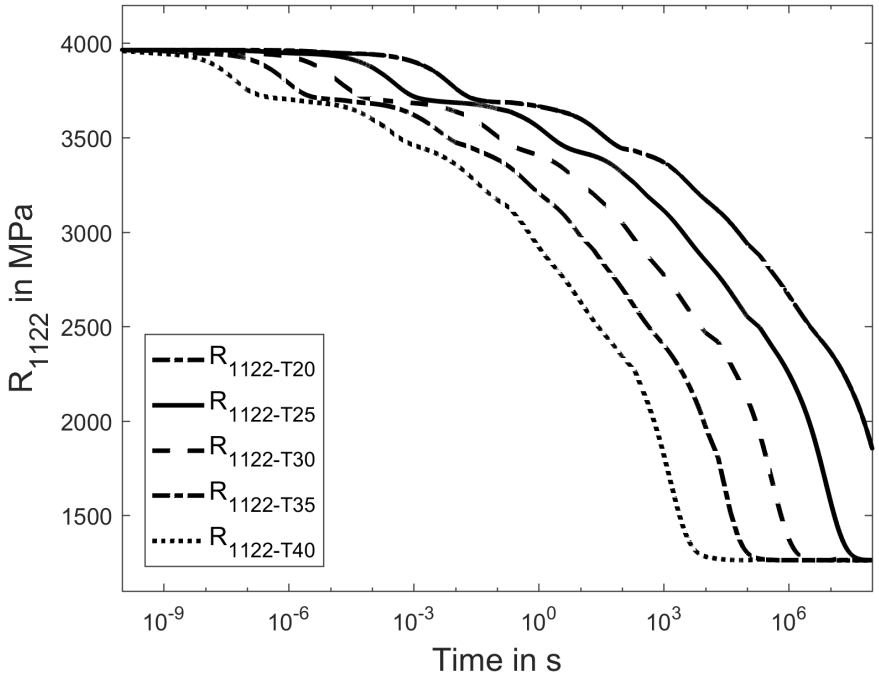


**Fig. 4.9:** Development of relaxation tensor entry $R_{1122}$ of the composite over a logarithmic time scale at 20, 25, 30, 35 and 40°C

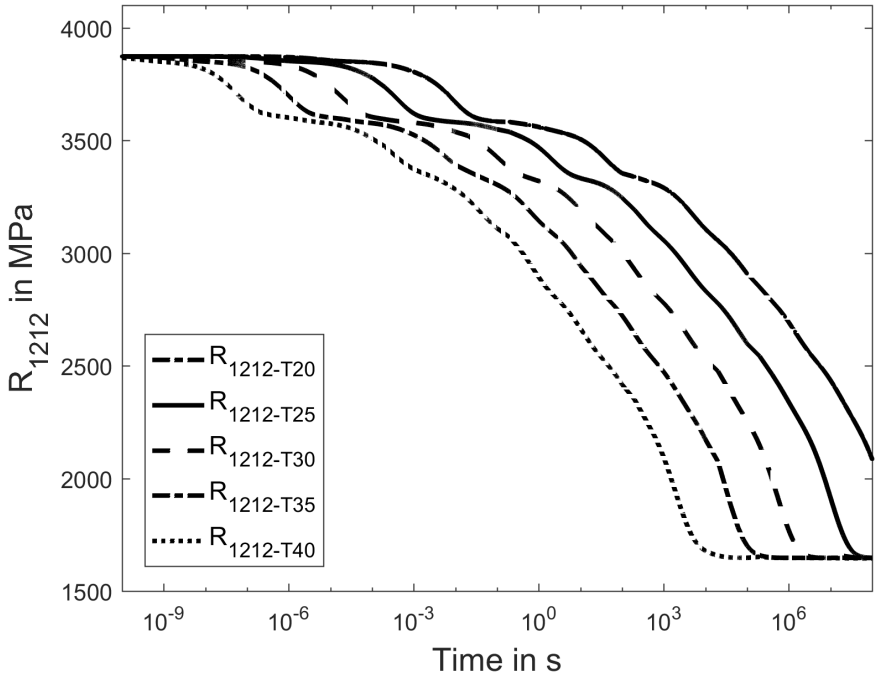


**Fig. 4.10:** Development of relaxation tensor entry $R_{1212}$ of the composite over a logarithmic time scale at 20, 25, 30, 35 and 40°C

## 4.2 Time-temperature-behaviour

In the following the shifted relaxation curves are only presented in the figures for a reference temperature of 30°C and without the relaxation curves at 20°C for a better clarity. The determined shifting parameters of the composite are listed for a comparison in tables at all chosen reference temperatures.

### 4.2.1 Shift function fitted for material tensor entry $R_{1111}$

#### 4.2.1.1 Shifting parameters

The shifting parameters are determined for a shift fitted for the relaxation tensor entry $R_{1111}$ at a reference temperature of 20°C, 30°C and 40°C. Those shifting parameters are presented in table 4.6 for a WLF-shift function and an Arrhenius one. A comparison of the activation energies shows that these reduce for rising reference temperatures and rises for lower ones. Such a behaviour corresponds to literature. A similar behaviour is observed for the parameters of the WLF-shift function. The WLF-parameter $C_1$ lowers with higher reference temperatures whereas on the other hand the parameter $C_2$ rises.

#### 4.2.1.2 Shifted relaxation curves

The figures 4.11, 4.12, 4.13 and 4.14 are almost equivalent to the ones 4.7, 4.8, 4.9 and 4.10 respectively in terms of line styles and temperatures excepting the missing 20°C curve. Three additional curves are added to represent the shifted relaxation tensor entries at the temperatures 25, 35 and 40°C.

The relaxation tensor entry $R_{1111}$ is fitted with the WLF-shifting parameters according to table 4.6 for 30°C. The minimum, maximum and quadratic mean difference between the

**Tab. 4.6:** Comparison of the shifting parameters for a shift fitted for relaxation tensor entry $R_{1111}$ at different reference temperatures. The WLF-shifting parameters are determined by trial and error while the Arrhenius ones are obtained by fitting the Arrhenius shift function to the shifting factors determined by the WLF-shifting function

| | WLF | | Arrhenius |
|---|---|---|---|
| $T_{Ref}$ in °C | $C_1$ | $C_2$ | E in kJ mol$^{-1}$ |
| 20 | 75.5 | 131.7 | 418.5 |
| 30 | 70.2 | 141.7 | 385.9 |
| 40 | 65.6 | 151.7 | 365.2 |

shifted relaxation curves and the original ones are presented in table 4.7 for an overview. The WLF-shift results in an almost perfectly visual match for the curve pairs at 25°C. A similar behaviour is obtained for the original relaxation curve and the shifted one at 35°C. Both visually coincide almost completely whereas at a closer look a few minor deviations can be seen. At 40°C the shifted relaxation times are slightly bigger than the original ones but it still looks like an acceptable shift although both curves do not perfectly match. The mean deviation is also bigger than for the other two curve pairs.

The same shifting parameters are also used for the other relaxation tensor entries and the mean, minimum and maximum deviations are also presented in table 4.7. For the relaxation tensor entry $R_{2222}$ at 25°C the shifted and original curve are the closest in comparison to the other pairs of curves but their mismatch is obvious. The curve pair at 35°C is also close by but it also does not match. The difference between those two relaxation curves is greater than for the curve pair at 25°C. A comparison of the relaxation curves at 40°C results in an obviously not matching curve pair and their deviation is even higher.

At 25°C the original curve and the shifted one of the shear tensor entry $R_{1212}$ are the closest curve pair of all three but its mismatch is more than obvious. Similar results are obtained for the curves at 35°C which are less close by than the curve pair at 25°C and they deviate even more. The shifted relaxation curve and the original one at 40°C do not match in any way and their mismatch is the biggest of all three curve pairs. An overview of the calculated deviations are presented in table 4.7.

For both coupling tensor entries $R_{1122}$ and $R_{2211}$ the calculated deviations are equal and are presented in table 4.7 only for the $R_{1122}$-element. The curve pair at 25°C is also the closest one of all three ones but they visually mismatch. The shifted and the original relaxation curve at 35°C on the other hand mismatches even more whereas the biggest difference of the curve pairs occurs for the one at 40°C.

A comparison between the calculated deviations and the figures of the relaxation tensor entry $R_{1111}$ leads to a justified suspicion of a mislead deviation calculation.

**Tab. 4.7:** Overview of the calculated quadratic mean, minimum and maximum deviations between the shifted and original relaxation tensor entries for a shift fitted for relaxation tensor entry $R_{1111}$ at a reference temperature of 30°C.

| | Temperature in °C | Min in % | Max in % | Mean in % |
|---|---|---|---|---|
| $R_{1111}$ | 25 | -31.55 | 8.18 | 12.31 |
| | 35 | 0.34 | 55.3 | 10.74 |
| | 40 | -19.7 | 163.79 | 53.06 |
| $R_{1122}$ | 25 | -48.05 | 1.76 | 25.79 |
| | 35 | -91.35 | 109.85 | 58.53 |
| | 40 | -11.86 | 227.43 | 176.54 |
| $R_{2222}$ | 25 | -47.87 | 1.92 | 25.26 |
| | 35 | -91.15 | 106.72 | 58.44 |
| | 40 | -17.33 | 259.64 | 175.25 |
| $R_{1212}$ | 25 | -43.36 | 2.76 | 24.04 |
| | 35 | -90.35 | 88.78 | 54.84 |
| | 40 | -11.86 | 227.43 | 163.61 |

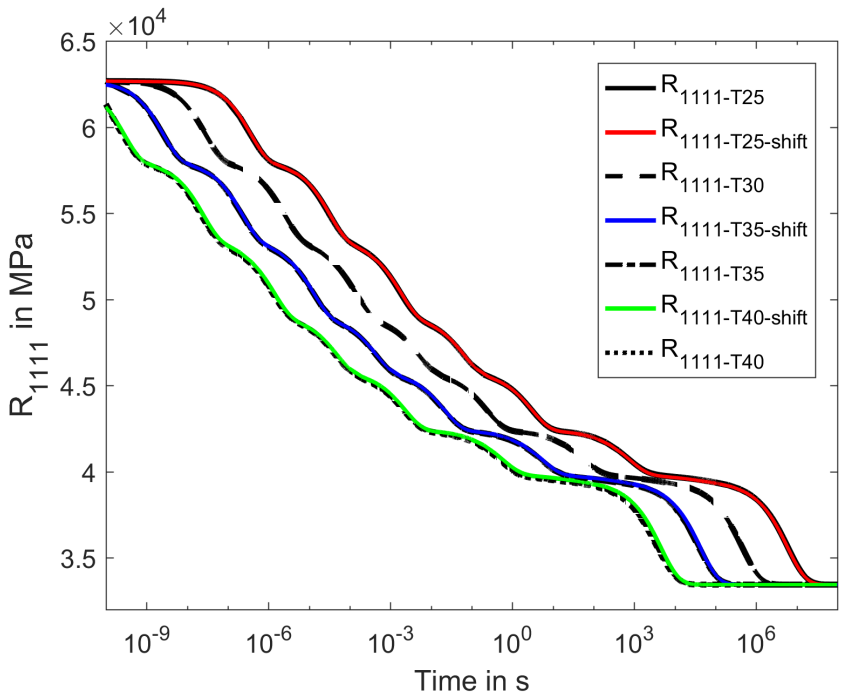


**Fig. 4.11:** Relaxations curves of tensor entry $R_{1111}$ shifted from 30°C to the original ones at 25, 35 and 40°C by the use of the WLF-shift function fitted for tensor entry $R_{1111}$.

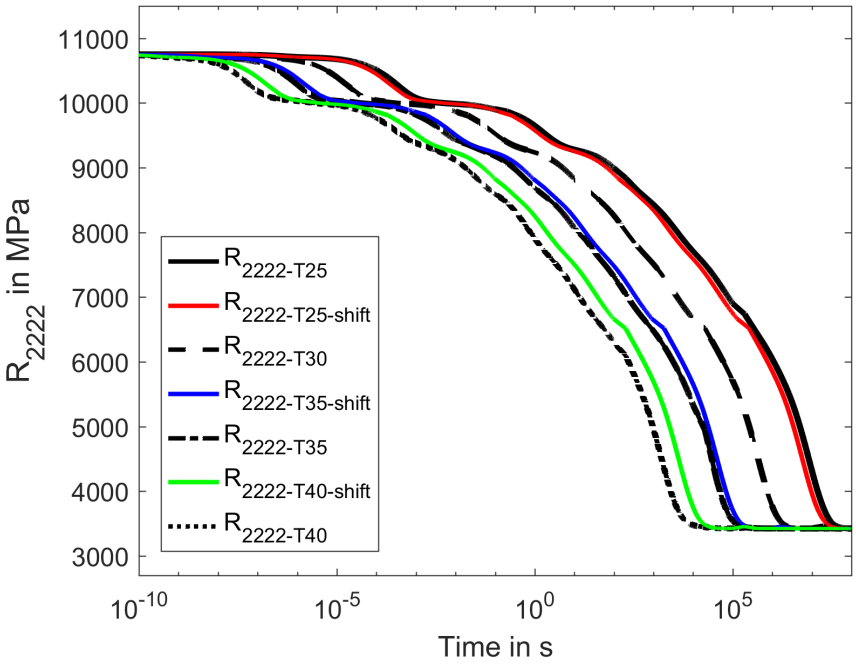


**Fig. 4.12:** Relaxations curves of tensor entry $R_{2222}$ shifted from 30°C to the original ones at 25, 35 and 40°C by the use of the WLF-shift function fitted for tensor entry $R_{1111}$.

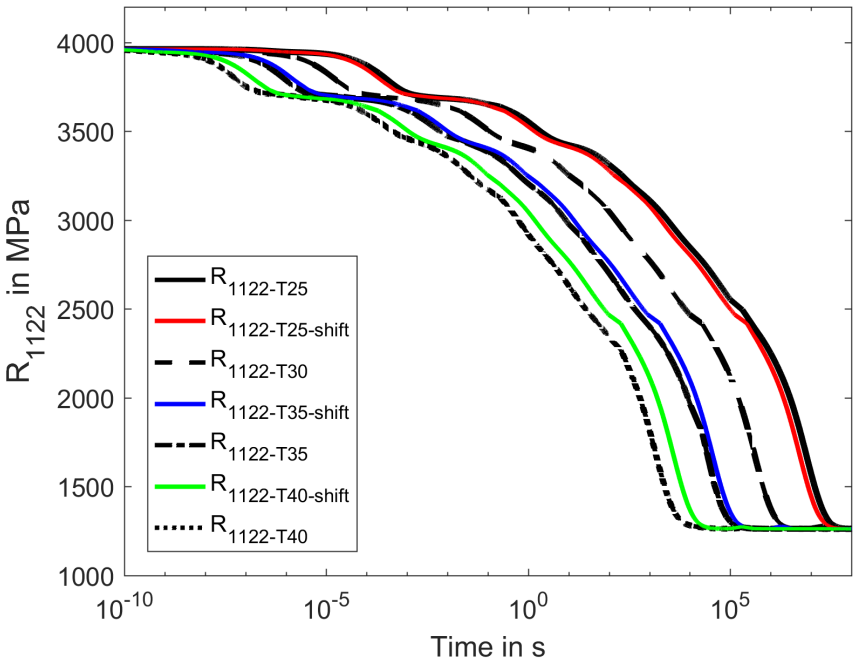


**Fig. 4.13:** Relaxations curves of tensor entry $R_{1122}$ shifted from 30°C to the original ones at 25, 35 and 40°C by the use of the WLF-shift function fitted for tensor entry $R_{1111}$.

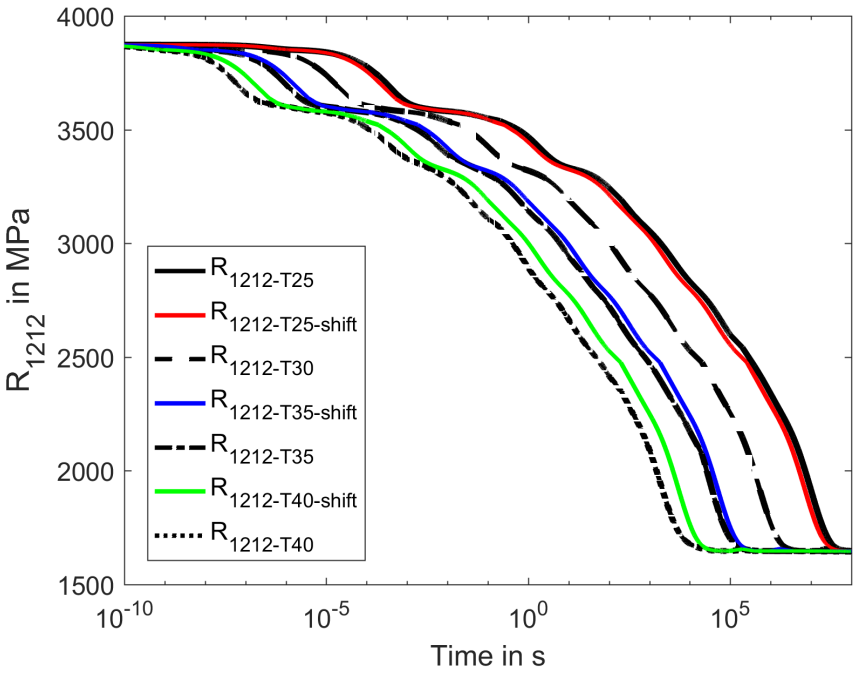


**Fig. 4.14:** Relaxations curves of tensor entry $R_{1212}$ shifted from 30°C to the original ones at 25, 35 and 40°C by the use of the WLF-shift function fitted for tensor entry $R_{1111}$.

#### 4.2.1.3 Correcting the calculation of the quality measure

Plotting the individual quality measures of the relaxation curve at 35°C over the time steps of the original relaxation curve shows fluctuating quality measures which are presented in figure 4.15. The highest peak of the quality measure is caused by the distinctive flat spot. This section strongly affects the calculation of the mean deviation and distorts it to higher values. Correcting this error by excluding this region from the calculation eliminates most of the unreasonable high values. This also applies to the other relaxations curves of the $R_{1111}$-element in similar way and therefore they are individually excluded from the calculation. The table 4.8 lists the new time intervals for the corrected calculation. It leads to new mean, minimum and maximum deviations for all curves which are displayed in table 4.9.

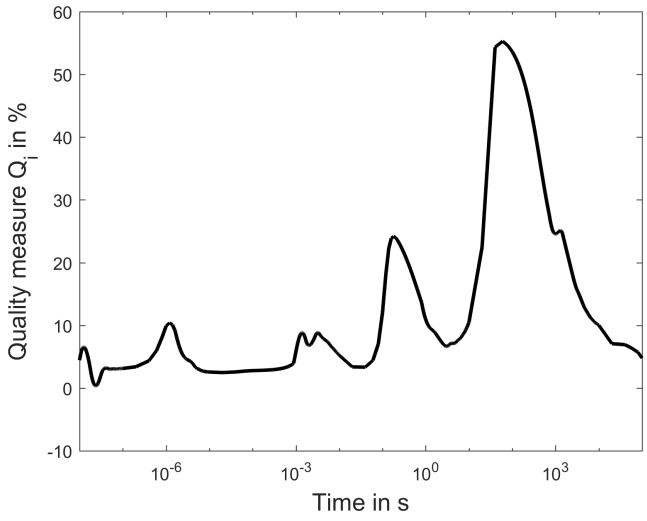


**Fig. 4.15:** Individual quality measures of the relaxation tensor entry $R_{1111}$ over the time steps of the original relaxation curve at 35°C. The highest peak is caused by the plateau region.

**Tab. 4.8:** Listing of the new sub-intervals used for the corrected quality measure calculation

| $T$ in °C | corrected sub-intervals in s | |
|---|---|---|
| 25 | $[9.8 \cdot 10^{-8}\ 3 \cdot 10^{4}]$ | $[1 \cdot 10^{5}\ 3 \cdot 10^{7}]$ |
| 35 | $[2 \cdot 10^{-9}\ 10]$ | $[9 \cdot 10^{3}\ 2 \cdot 10^{5}]$ |
| 40 | $[2 \cdot 10^{-9}\ 0.1]$ | $[1 \cdot 10^{2}\ 1.2 \cdot 10^{4}]$ |

**Tab. 4.9:** Overview of the corrected mean, minimum and maximum deviations between the shifted and original relaxation tensor entries for a shift fitted for relaxation tensor entry $R_{1111}$ and at a reference temperature of 30°C.

| | Temperature in °C | Min in % | Max in % | Mean in % |
|---|---|---|---|---|
| $R_{1111}$ | 25 | -31.55 | 8.18 | 8.79 |
| | 35 | -25.02 | 24.18 | 7.12 |
| | 40 | 8.65 | 67.95 | 28.44 |
| $R_{1122}$ | 25 | -48.05 | 1.77 | 24.07 |
| | 35 | -24.64 | 78.18 | 53.33 |
| | 40 | 16.24 | 220.6 | 161.28 |
| $R_{2222}$ | 25 | -47.87 | 1.92 | 23.79 |
| | 35 | -22.76 | 77.20 | 53.33 |
| | 40 | 15.80 | 219.23 | 160.50 |
| $R_{1212}$ | 25 | -43.36 | 2.76 | 22.22 |
| | 35 | -18.03 | 68.27 | 50.10 |
| | 40 | 13.32 | 206.16 | 150.62 |

#### 4.2.1.4 Further remarks

The overall TTS-behaviour is thermorheoligcally complex which results from the mismatches of the shifts for the majority of the relaxation tensor entries. Some changes of curvature can also be seen in certain sections of the curve development but they are small for this material combination. According to the pre-defined requirement in terms of shift quality the shifts of the relaxation tensor entry $R_{1111}$ are only acceptable for the curve pairs at 25°C and 35°C while the shift at 40°C is on average above the ten percent limit. It is mentioned that this fitted shift is not suitable for the rest of the relaxation tensor entries. A comparison between the shifted relaxation times and the original ones results in faster times for the shifted curves at 25°C and on the other hand, in slower times for the shifted ones at 35°C and 40°C. This shifting behaviour shows that the determined shifting

**Tab. 4.10:** Comparison of the shifting parameters for a shift fitted for relaxation tensor entry $R_{2222}$ at different reference temperatures. The WLF-shifting parameters are determined by trial and error while the Arrhenius ones are obtained by fitting the Arrhenius shift function to the shifting factors determined by the WLF-shifting function

| | WLF | | Arrhenius |
|---|---|---|---|
| $T_{Ref}$ in °C | $C_1$ | $C_2$ | E in kJ mol$^{-1}$ |
| 20 | 106.7 | 164.5 | 470 |
| 30 | 100.6 | 174.5 | 446 |
| 40 | 95.2 | 184.5 | 430 |

parameters are not so exact and the true ones might be a bit higher. Similar results are obtained by an Arrhenius shift with an activation energy according to table 4.6 for 30°C.

## 4.2.2 Shift function fitted for material tensor entry $R_{2222}$

### 4.2.2.1 Shifting parameters

The shifting parameters are determined for a shift fitted for the relaxation tensor entry $R_{2222}$ at a reference temperature of 20°C, 30°C and 40°C. Those shifting parameters are presented in table 4.10 for a WLF-shift function and an Arrhenius one. A comparison of the activation energies and of the WLF-shifting parameters shows the same characteristics as for the shift fitted for relaxation tensor entry $R_{1111}$.

### 4.2.2.2 Shifted relaxation curves

The figures 4.16, 4.17, 4.18 and 4.19 are also equivalent to the above figures 4.7, 4.8, 4.9, 4.10 respectively in terms of line styles and temperatures excepting the missing 20°C curve. Additional continuous red, blue and green lines are used to represent three shifted relaxation curves for 25, 35 and 40°C, respectively.

For the relaxation tensor entry $R_{2222}$ the WLF-shifting parameters according to table 4.10 result in a good conformity for the curve pair at 25°C excepting the little misfit of the kink at $2 \cdot 10^5$s. Those two curves deviate from each other on average according to table 4.11 in which also the minimum and maximum deviations are presented. For the original and the shifted relaxation curve at 35°C a similar behaviour is achieved although a few but small misfits can be seen. At 40°C the shifted curve has bigger relaxation times than the original relaxation curve and but a changing in curvature is more apparent.

At 25°C the shifted curve of the shear tensor entry largely coincides with the original relaxation curve excepting the little kink at $2 \cdot 10^5$s. The curve pair at 35°C visually coincide for a majority and look like a quite good shift even they deviate in a few areas. In contrary to this, the original and the shifted relaxation curve at 40°C differ for a majority from each other. Small changes in curvature can also be seen at the transition state before equilibrium. The deviations of those curve pairs are presented in the table 4.11.

The curve pair of the symmetric coupling tensor entries $R_{1122}$ and $R_{2211}$ and their deviations are equal and so the deviations between the shifted and original relaxation curves are presented only for the $R_{1122}$-element in table 4.11. The shifted and the original relaxation curve at 25°C result in an almost perfect match also excepting the mismatch of the kinks at about $3 \cdot 10^5$s. At 35°C the shifted relaxation curve is also close to the original one and they match for a large range. A few differences can be seen in some sections. Both relaxation curves at 40°C look like an inappropriate shift due to visually distinct differences. Its difference gets more evident especially the change in curvature before the equilibrium state.

The relaxation tensor entry $R_{1111}$ is also shifted by the same shifting parameters and the calculated deviations are also presented in table 4.11. The original and the shifted relaxation curve at 25°C are close together but they do not fit. In general the shifted relaxation times are bigger than the original ones. At 35° both curves do not match either but those are the closest of all three curve pairs. In opposite to the relaxation times of the pair at 25°C the shifted times at 35°C are smaller. The original and the shifted relaxation curve at 40°C are obviously not matching and the misfit is even higher in comparison to the other two curve pairs.

When comparing the calculated deviations and the figures for the relaxation tensor entries $R_{2222}$, $R_{1122}$ and $R_{1212}$, it seems that the shifts visually fit better than the calculated values predict.

**Tab. 4.11:** Overview of the calculated mean, minimum and maximum deviations between the shifted and original relaxation tensor entries for a shift fitted for relaxation tensor entry $R_{2222}$ at a reference temperature of 30°C.

| | Temperature in °C | Min in % | Max in % | Mean in % |
|---|---|---|---|---|
| $R_{1111}$ | 25 | 2.11 | 61.37 | 44.68 |
| | 35 | -94.21 | 3.11 | 32.44 |
| | 40 | -64.81 | 15.60 | 41.85 |
| $R_{1122}$ | 25 | -22.51 | 51.93 | 19.50 |
| | 35 | -44.67 | 39.32 | 9.45 |
| | 40 | -49.06 | 59.96 | 28.07 |
| $R_{2222}$ | 25 | -22.24 | 52.02 | 20.31 |
| | 35 | -45. | 37.25 | 9.42 |
| | 40 | -49.25 | 57.6 | 27.70 |
| $R_{1212}$ | 25 | -15.51 | 53.29 | 23.82 |
| | 35 | -43.43 | 25.34 | 8.45 |
| | 40 | -50.34 | 43.49 | 24.18 |

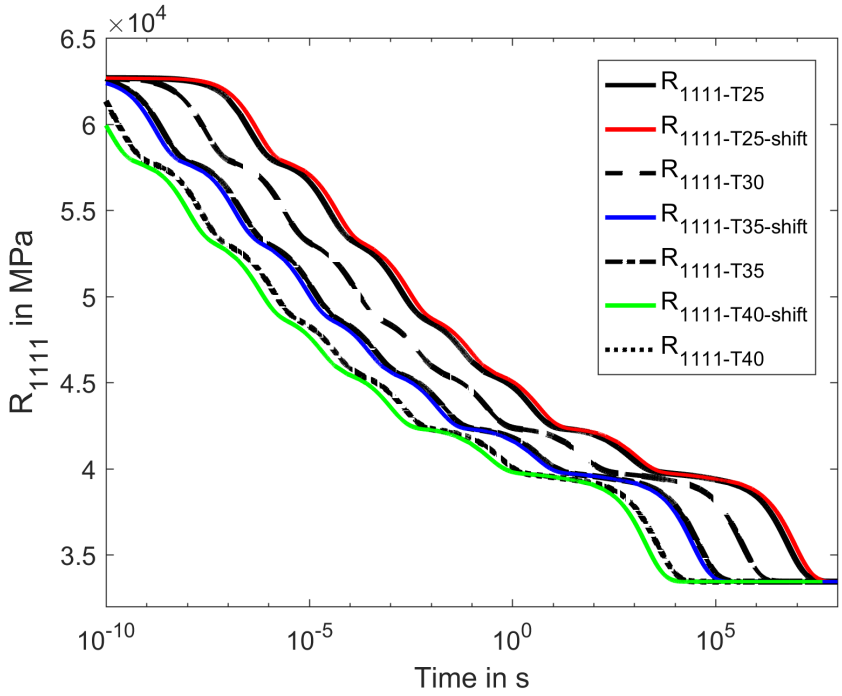


**Fig. 4.16:** Relaxations curves of tensor entry $R_{1111}$ shifted from 30°C to the original ones at 25, 35 and 40°C by the use of the WLF-shift function fitted for tensor entry $R_{2222}$.

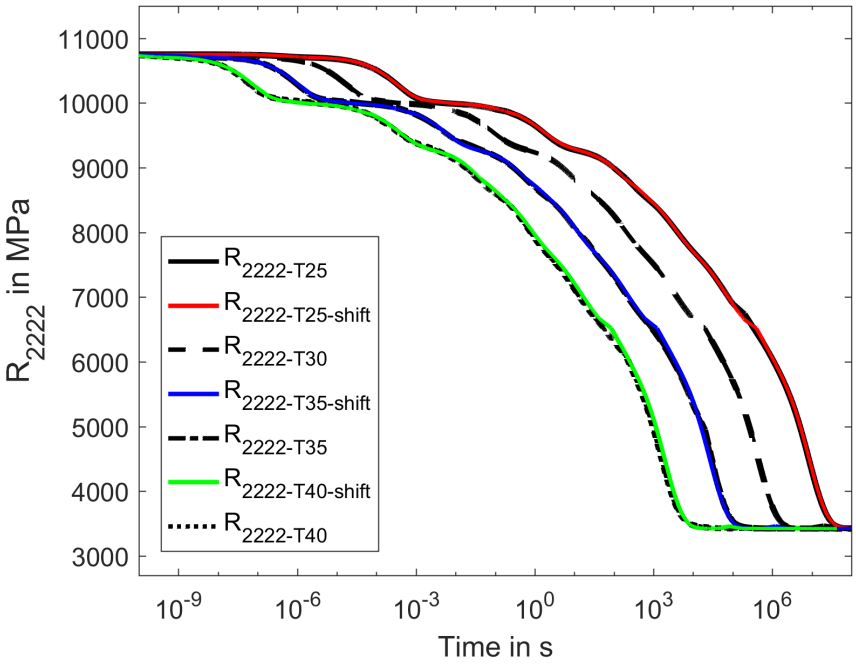


**Fig. 4.17:** Relaxations curves of tensor entry $R_{2222}$ shifted from 30°C to the original ones at 25, 35 and 40°C by the use of the WLF-shift function fitted for tensor entry $R_{2222}$.

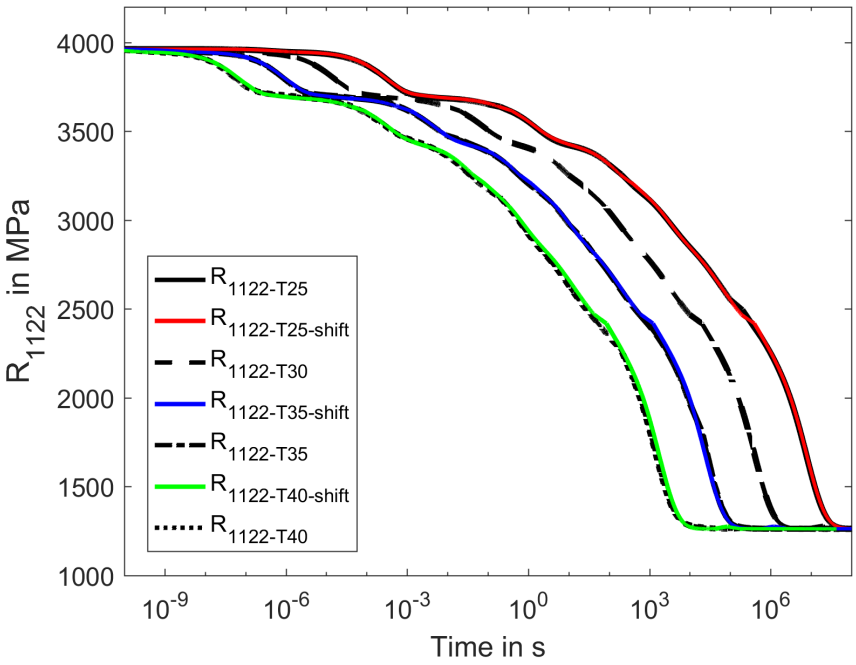


**Fig. 4.18:** Relaxations curves of tensor entry $R_{1122}$ shifted from 30°C to the original ones at 25, 35 and 40°C by the use of the WLF-shift function fitted for tensor entry $R_{2222}$.

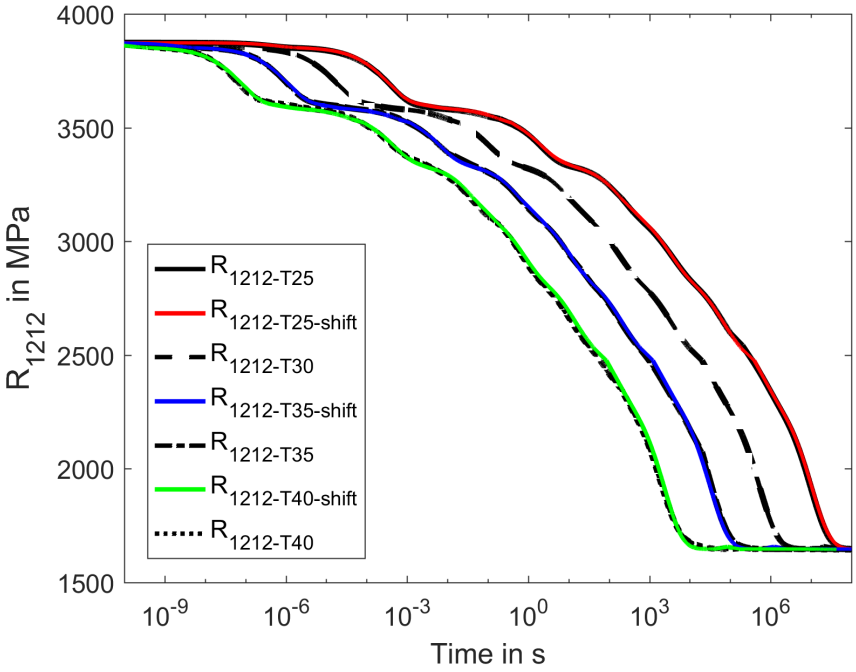


**Fig. 4.19:** Relaxations curves of tensor entry $R_{1212}$ shifted from 30°C to the original ones at 25, 35 and 40°C by the use of the WLF-shift function fitted for tensor entry $R_{2222}$.

#### 4.2.2.3 Correcting the calculation of the quality measure

The individual quality measures are also used for the correction of the quality measure calculation. Therefore the individual quality measures of the relaxation curve $R_{2222}$ at 35°C are plotted against the time steps of the original relaxation curve. The fluctuating quality measures are presented in figure 4.20. The flat spot between approximately $1 \cdot 10^{-6}$s and $2 \cdot 10^{-4}$s causes one of the strongest peak downwards and this area also strongly affects the calculated values. The already mentioned kink at $1.2 \cdot 10^{3}$s also affects the mean deviation. Therefore these areas are excluded from the calculation and the new time intervals for determining the quality measures are presented in table 4.12. The same is also applied in a similar way to the other relaxation curves. This change leads to new deviations which are presented in table 4.13.

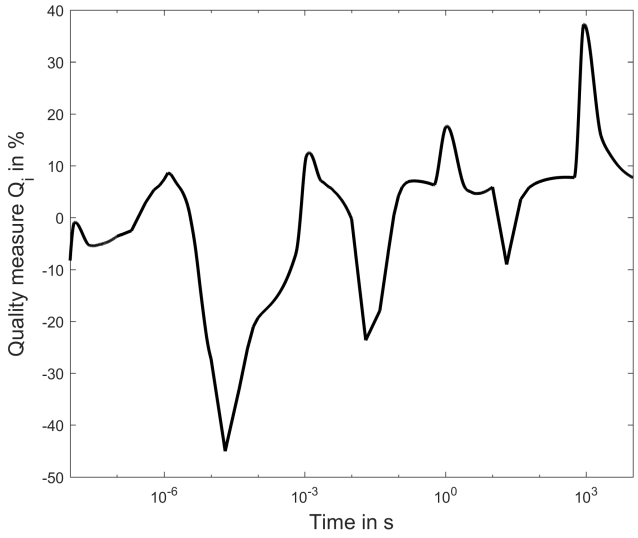


**Fig. 4.20:** Individual quality measures over the time steps of the original relaxation curve $R_{2222}$ at 35°C. Highest peaks are caused by the plateau region and by the kink.

**Tab. 4.12:** Listing of the new sub-intervals used for the corrected quality measure calculation

| $T$ in °C | corrected sub-intervals in s | | |
|---|---|---|---|
| 25 | $[1 \cdot 10^{-5}\ 9 \cdot 10^{-5}]$ | $[10\ 9 \cdot 10^{4}]$ | $[1 \cdot 10^{7}\ 3 \cdot 10^{7}]$ |
| 35 | $[8 \cdot 10^{-9}\ 3 \cdot 10^{-6}]$ | $[7 \cdot 10^{-4}\ 7 \cdot 10^{2}]$ | $[2 \cdot 10^{3}\ 1 \cdot 10^{4}]$ |
| 40 | $[2 \cdot 10^{-9}\ 1 \cdot 10^{-7}]$ | $[4 \cdot 10^{-5}\ 40]$ | $[80\ 2 \cdot 10^{3}]$ |

**Tab. 4.13:** Overview of the mean, minimum and maximum deviations between the shifted and the original relaxation tensor entries for a shift fitted for relaxation tensor entry $R_{2222}$ and at a reference temperature of 30°C.

| | Temperature in °C | Min in % | Max in % | Mean in % |
|---|---|---|---|---|
| $R_{1111}$ | 25 | 2.11 | 53.98 | 37.57 |
| | 35 | -33.38 | 3.11 | 28.29 |
| | 40 | -52.39 | 15.60 | 41.59 |
| $R_{1122}$ | 25 | -7.03 | 51.81 | 9.8 |
| | 35 | -25.55 | 23.32 | 7.1 |
| | 40 | -20.02 | 50.17 | 23.59 |
| $R_{2222}$ | 25 | -6.80 | 52.02 | 9.86 |
| | 35 | -23.64 | 21.45 | 7.13 |
| | 40 | -20.06 | 49.04 | 23.41 |
| $R_{1212}$ | 25 | -3.19 | 23 | 7.98 |
| | 35 | -23.34 | 13.6 | 6.5 |
| | 40 | -25.31 | 39.96 | 20.46 |

#### 4.2.2.4 Further remarks

As already mentioned the overall TTS-behaviour is thermorheoligcally complex. In some sections it is possible to identify changes of curvature. However, those changes are small for this material combination. Checking the shift quality with the pre-defined requirement of ten percent quadratic mean deviation shows that the shifts of relaxation tensor entry $R_{2222}$ are only acceptable for 25°C and 35°C but not for 40°C. The same applies to the shifts of the coupling and shear tensor entries. It is mentioned that the fitted shifts of relaxation tensor $R_{2222}$ are not suitable for shifts for relaxation tensor entry $R_{1111}$. A comparison between the shifted relaxation times and the original ones generally results in slower times for the shifted curves of the relaxation tensor entries $R_{2222}$, $R_{1122}$ and $R_{1212}$ at all temperatures. The shifted relaxation times for the relaxation tensor entry $R_{1111}$ are slower at 25°C whereas they are faster at 35°C and 40°C in comparison to the

original times. This shifting behaviour shows that the determined shifting parameters are acceptable but they are to big for the relaxation tensor entry $R_{1111}$. An equivalent result can be obtained by an Arrhenius shift with an activation energy according to table 4.10 for 30°C.

### 4.2.3 Comparison of TTS-parameters

The first impression of the TTS-behaviour is misleading and the present composite can not be considered as fully thermorheologically simple. Thus the TTS behaviour is instead considered as thermorheologically complex but for a small temperature range the assumption of an direction dependent thermorheologically simple material is permissible. The range of temperatures for such direction dependent thermorheologically simple composites depends on the allowable quality measure. Such a direction dependent thermorheological material behaviour might be caused by the composites constituents and their individual relaxation behaviour especially the combination of their characteristic times of the Prony terms.

The shifting parameters of the composite's constituents and the determined ones are compared for the relaxation tensor entries $R_{1111}$ and $R_{2222}$ to identify the dominance of either matrix or fibre in terms of the overall TTS behaviour. The figures 4.21, 4.22, 4.23 and 4.24 display the relaxation tensor entries $R_{1111}$, $R_{2222}$, $R_{1122}$ and $R_{1212}$ over time at 20°C, 30° and 40°C, respectively. The relaxation curves at 20°C are now shifted with the shift parameters of the matrix whereas the ones at 40°C are shifted with the shift parameters of the fibre. Both are shifted to a target temperature of 30°C. A blue and a red line colour represent the matrix's parameter shifted relaxation curve and the fibre's parameter shifted one in the figures, respectively. The quality measures are also corrected similar to the sections 4.2.1.3 and 4.2.2.3 and the used time intervals are presented for the quality measure calculation in table 4.14.

The shifting parameters of the matrix lead to a shift which is surprisingly closer to the target temperature of 30°C for the relaxation tensor entry $R_{1111}$ than the one which is shifted with the parameters of the fibre. The mean deviation between the original relaxation curve and the matrix's parameter shifted one is still about 51.84% whereas the one shifted with fibre's parameters deviates about 94.26%. The matrix is also more dominant for the relaxation tensor entry $R_{2222}$ and the difference between the shifted relaxation curve and the original one amounts on average about 7.81%. On the other hand, the fibre's parameter shifted curve medially deviates about 96.94%. The same applies to the coupling and shear tensor entry who are also dominated more by the matrix than the fibre in terms of the TTS behaviour. Similar mean deviations occur for the coupling and shear tensor entries. All corrected deviations are listed for an overview in table 4.15.

Such a behaviour can be derived from the difference between the activation energies of the composite's constituents. The activation energy of the fibre is a little bit more than 38% of the matrix's one at 20°C which leads to a less sensitive behaviour of the fibre to temperature and thus the matrix becomes the dominant part in terms of the TTS behaviour for relaxation tensor entry $R_{1111}$. To fit the shifts for this relaxation tensor entry the activation energy of the matrix needs to be decreased to the already determined one in table 4.6 at 20°C which is about 6.6% lower. On the other hand, the converted activation energy of the fibre needs to be increased to the determined ones in table 4.6 at 40°C which is about 222% higher. The dominant part is the matrix for the TTS behaviour of the relaxation tensor entry $R_{2222}$ which results in an almost perfect shift. The determined activation energies of the composite and the matrix's one are of the same order and they deviate less than two per cent from each other at the same reference temperature. This also applies to the shear and coupling tensor entry in an analogue way.

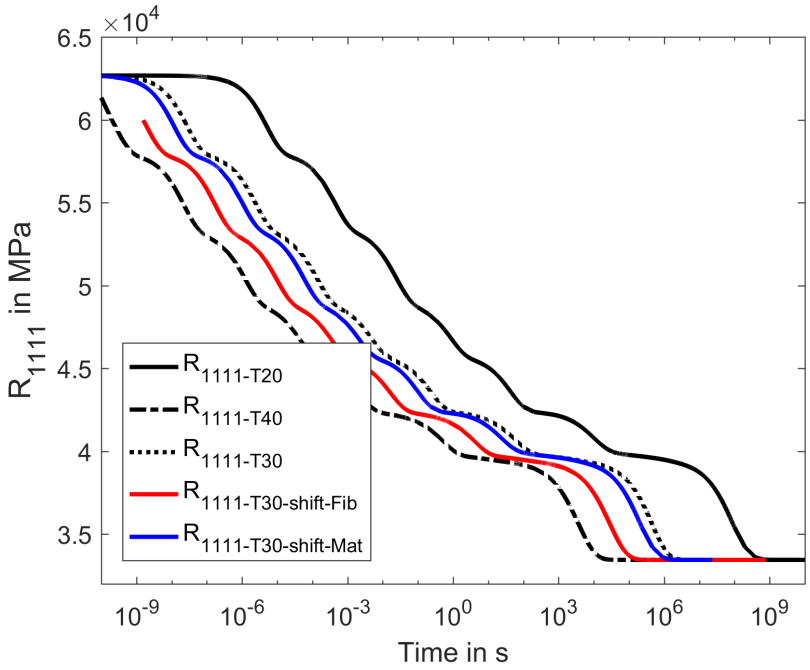


**Fig. 4.21:** Relaxation tensor entry $R_{1111}$ at the temperatures 20, 30 and 40°C. The relaxation curves at 20 and 40°C are shifted with the shifting parameters of matrix and fibre to the curve at 30°C respectively.

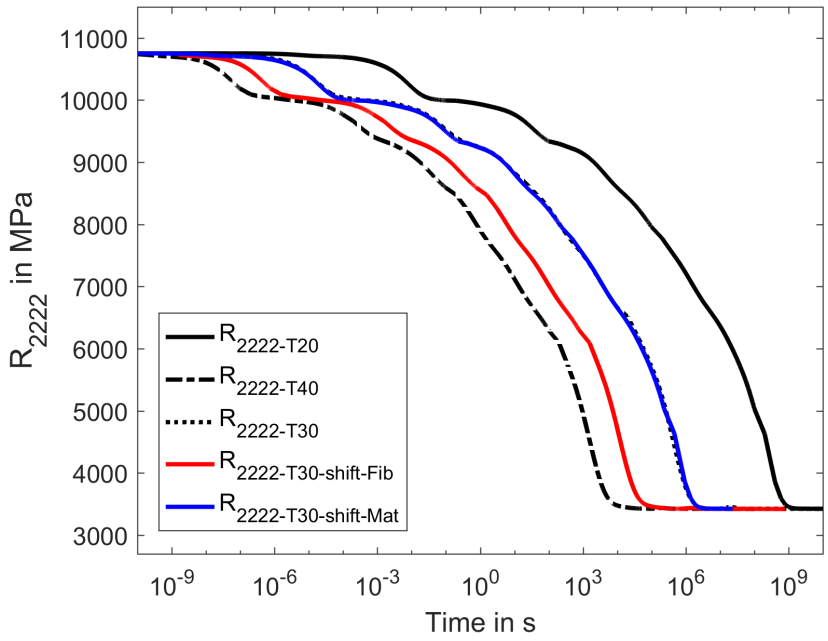


**Fig. 4.22:** Relaxation tensor entry $R_{2222}$ at the temperatures 20, 30 and 40°C. The relaxation curves at 20 and 40°C are shifted with the shifting parameters of matrix and fibre to the curve at 30°C respectively.

**Tab. 4.14:** Listing of the new sub-intervals used for the corrected quality measure calculation

| | Tensor entry | corrected sub-intervals in s | |
|---|---|---|---|
| Fibre | $R_{1111}$ | $[4 \cdot 10^{-3}\ 9]$ | $[9 \cdot 10^{3}\ 3 \cdot 10^{6}]$ |
| | other | $[4 \cdot 10^{-3}\ 3 \cdot 10^{6}]$ | |
| Matrix | $R_{1111}$ | $[3 \cdot 10^{-8}\ 9]$ | $[5 \cdot 10^{3}\ 3 \cdot 10^{6}]$ |
| | other | $[1 \cdot 10^{-5}\ 4 \cdot 10^{-4}]$ | $[1\ 3 \cdot 10^{6}]$ |

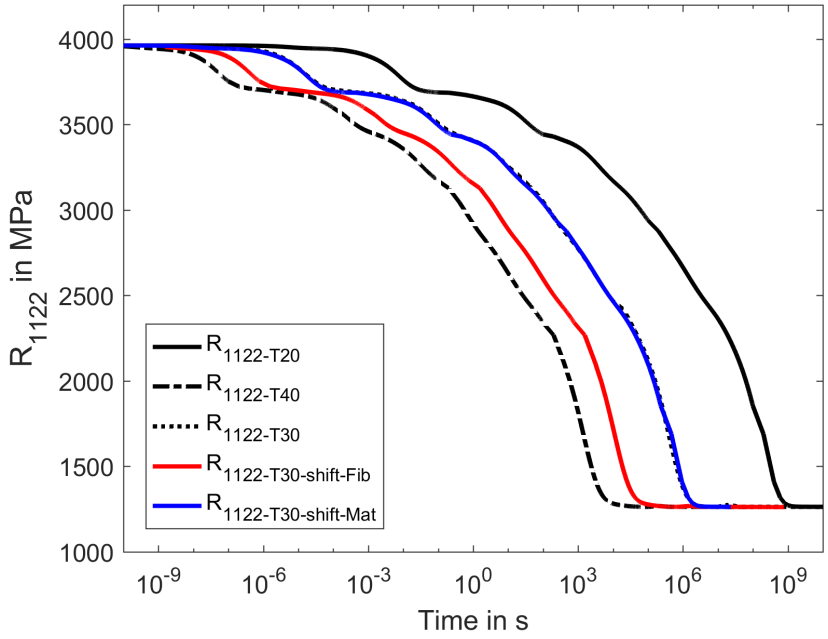


**Fig. 4.23:** Relaxation tensor entry $R_{1122}$ at the temperatures 20, 30 and 40°C. The relaxation curves at 20 and 40°C are shifted by the shifting parameters of the matrix and fibre to the curve at 30°C respectively.

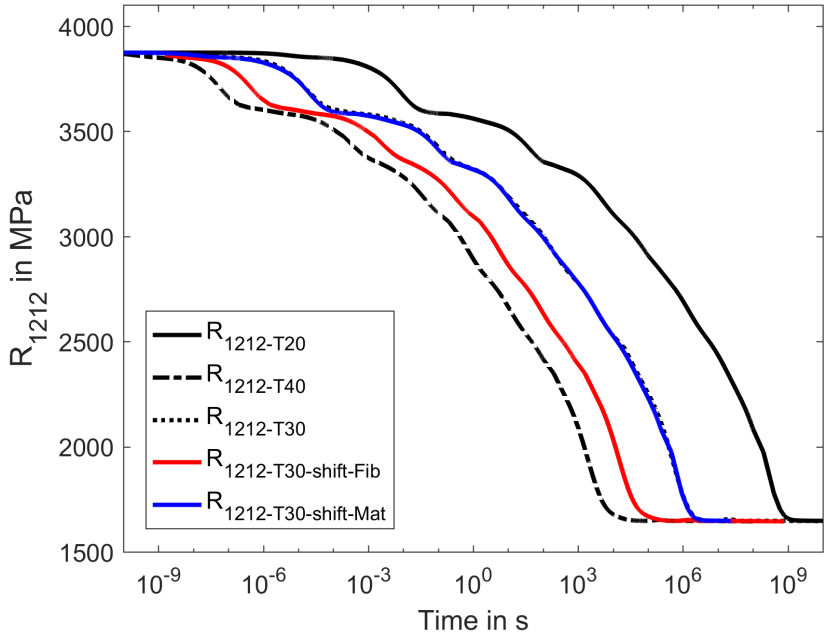


**Fig. 4.24:** Relaxation tensor entry $R_{1212}$ at the temperatures 20, 30 and 40°C. The relaxation curves at 20 and 40°C are shifted by the shifting parameters of the matrix and fibre to the curve at 30°C respectively.

**Tab. 4.15:** Overview of the mean, minimum and maximum deviations between the original relaxation curve at 30°C and the constituent's parameter shifted relaxation curves

| | Shifting parameters | Min in % | Max in % | Mean in % |
|---|---|---|---|---|
| $R_{1111}$ | Fibre | -95.82 | -93.18 | 94.26 |
| | Matrix | -58.08 | -28.49 | 51.84 |
| $R_{1122}$ | Fibre | -97.92 | -95.40 | 96.94 |
| | Matrix | -55.77 | 20.74 | 7.85 |
| $R_{2222}$ | Fibre | -97.88 | -95.61 | 96.94 |
| | Matrix | -55.88 | 21.89 | 7.81 |
| $R_{1212}$ | Fibre | -97.68 | -95.12 | 96.8 |
| | Matrix | -56.71 | 10.25 | 8.19 |

### 4.2.4 Changing the TTS-parameters of the fibre

To verify the effects of both individual TTS behaviours on the composites ones, the WLF-shifting parameters of the fibre are arbitrarily set to 79 and 175 at a reference temperature of 40°C which corresponds to an equivalent activation energy of 417.6 kJmol$^{-1}$ at 20°C. The activation energy of the matrix remains unchanged. At 20°C the equivalent activation energy of the fibre is still about 6.8% lower than the one of the matrix. The figures 4.25, 4.26, 4.28 and 4.27 present the relaxation tensor entries $R_{1111}$, $R_{2222}$, $R_{1122}$ and $R_{1212}$ over time at 20, 30 and 40°C, respectively.

Apparently the TTS behaviour is now neither dominated by the matrix nor by the fibre for the relaxation tensor entry $R_{1111}$. The spacing between the relaxation curves gets larger and the changes in curvature are more noticeable and severe. It can be assumed that this TTS behaviour is a function of the individual shifting parameters of fibre and matrix but also of time.

The TTS-behaviours of the remaining relaxation tensor entries are still dominated by the matrix. The changes in curvature are now more apparent in the region between $1 \cdot 10^{-4}$s and $1 \cdot 10^{4}$s for the relaxation tensor entry $R_{2222}$. This also applies to the coupling and especially to the shear tensor entry which has a stronger change of curvature.

Reviewing the changes of the fibre's parameters in comparison to the unchanged ones, it can be assumed that if the activation energy of the matrix is much higher than the one of the fibre it is possible to approximate the overall TTS-behaviour by the one of the matrix. On the other hand the TTS behaviour of the remaining relaxation tensor entries is still clearly dominated by the matrix before as well as after the change but the changes of curvature are more noticeable. Therefore it is permissible to approximate the overall TTS behaviour by the one of the matrix for the relaxation tensor entries $R_{2222}$, $R_{1122}$ and $R_{1212}$ but changes of curvature affect the shift's accuracy.

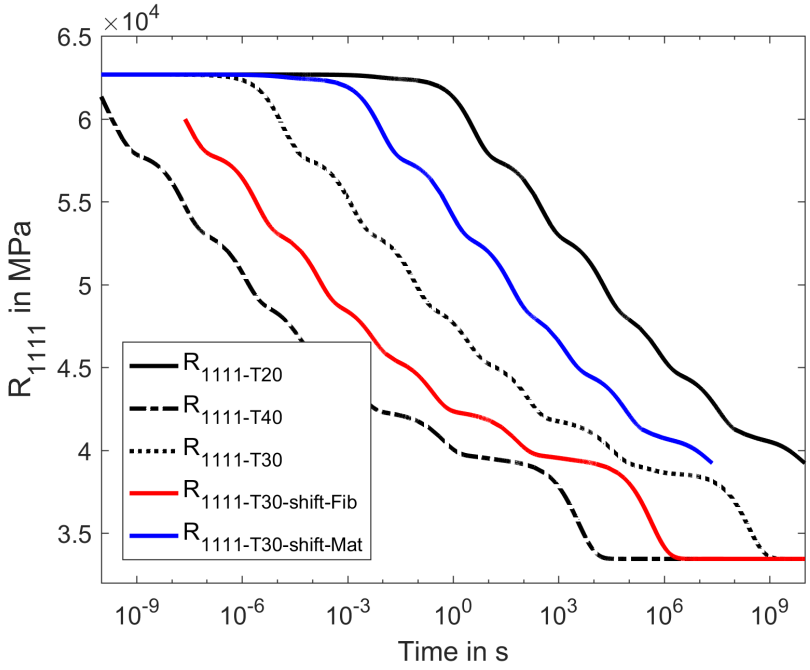


**Fig. 4.25:** Relaxation tensor entry $R_{1111}$ at the temperatures 20, 30 and 40°C. The relaxation curves at 20 and 40°C are shifted with the shifting parameters of the matrix and the changed ones of the fibre to 30°C.

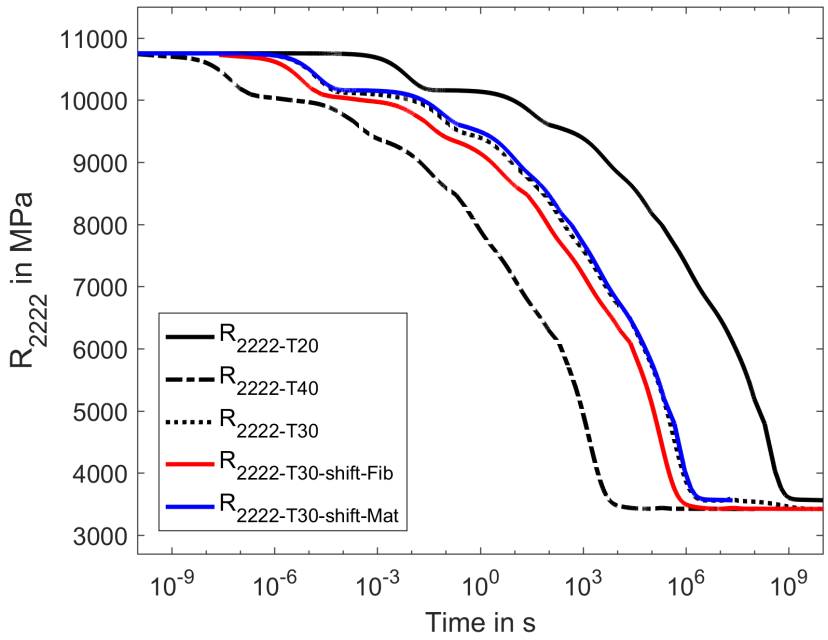


**Fig. 4.26:** Relaxation tensor entry $R_{2222}$ at the temperatures 20, 30 and 40°C. The relaxation curves at 20 and 40°C are shifted with the shifting parameters of the matrix and the changed ones of the fibre to 30°C.

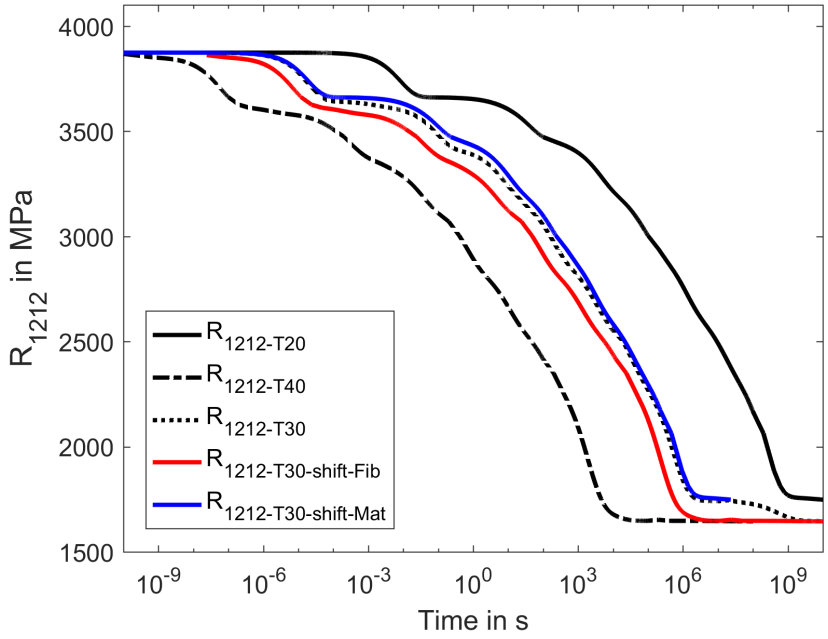


**Fig. 4.27:** Relaxation tensor entry $R_{1212}$ at the temperatures 20, 30 and 40°C. The relaxation curves at 20 and 40°C are shifted with the shifting parameters of the matrix and the changed ones of the fibre to 30°C.

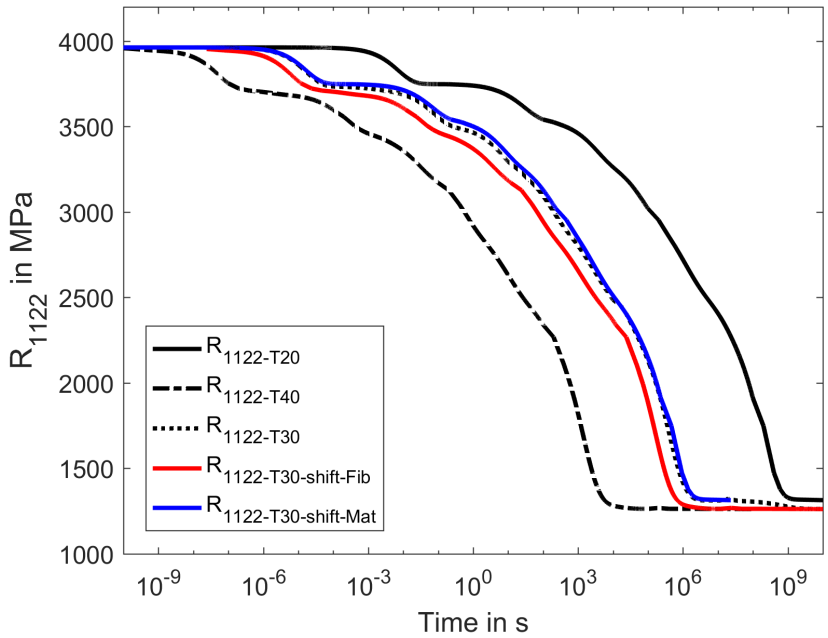


**Fig. 4.28:** Relaxation tensor entry $R_{1122}$ at the temperatures 20, 30 and 40°C. The relaxation curves at 20 and 40°C are shifted with the shifting parameters of the matrix and the changed ones of the fibre to 30°C.

# Chapter 5

# Conclusion

In this thesis a uni-directional fibre reinforced composite consisting of two different viscoelastic polymers is studied in terms of its macroscopic relaxation and its time-temperature shift behaviour. The periodic microfield approach is used to gain the material tensor entries of a thin ply and thus the composites macroscopic relaxation behaviour. A unit cell is used with periodic boundary conditions in form of a Finite Element representation in ABAQUS and it is subjected to load cases at different temperatures. The simulation results are further processed with the program MATLAB for a proper data analysis.

At a constant temperature the composite's material tensor entry $R_{1111}$ has a similar relaxation development over time as the pure fibre whereas the material tensor entry $R_{2222}$ has a similar development as the pure matrix. The coupling $R_{1122}$ and the shear tensor entry $R_{1212}$ are also similar to the development of the pure matrix. It can be said that the fibre is the dominant part for the material tensor entry $R_{1111}$ whereas the matrix takes up that place for the remaining material tensor entries in terms of relaxation. Such a behaviour corresponds to the literature in terms of mechanical properties. At first sight the composite's relaxation curves may imply thermorheoligcal simplicity due to similar looking curves which are equally spaced.

For this material combination a direction dependent shift is used whereby one shift is fitted for the material entry $R_{1111}$ and the second one is fitted for the material tensor entry $R_{2222}$ which also includes the coupling and shear relaxation tensor entry. Good fits can be achieved for each relaxation tensor entry at 25°C and also at 35°C although some deviations occur. Those are caused by slight changes of curvature in certain sections of development. The shifted curves at 40°C deviate too much on average from the original master curve and neither the shift fitted for the relaxation tensor entry $R_{1111}$ nor the one fitted for $R_{2222}$ satisfies the condition of thermorheoligcal simplicity. Therefore the composite has to be seen as thermorheologically complex but the assumption of a direction dependent thermorheoligcal simplicity is also acceptable for a certain temperature range,

although it does not fulfil this severe condition. A comparison of the shifting parameters between the pure matrix, the fibre and the composite shows a dominance of the matrix for the composite's overall TTS behaviour. This is due to a weaker sensibility of the fibre to temperature than the matrix in terms of shifting.

Increasing the fibre's TTS parameters in such a way that the TTS-behaviour of the fibre is of about the same order as the one of the matrix in terms of shifting. This leads to bigger temporal gaps in between the relaxation curves of the material tensor entry $R_{1111}$. There is no specific dominance of neither the fibre nor matrix. Therefore it can be stated that this TTS-behaviour composes from those ones of the composite's constituents but also depends on time. The matrix still dominates the composite's TTS behaviour for the remaining tensor entries but changes in curvature are more apparent in some sections. If the activation energy of the matrix is much higher than the one of the fibre at the same reference temperature, the macroscopic TTS-behaviour can be approximated by the one of the matrix for the material tensor entries.

In this thesis the gained knowledge of a composite consisting of two different viscoelastic materials is limited and only valid for the present material combination. The current outcome shows that if the composite is labelled as thermorheoligcally complex, there can be even a certain combination of viscoelastic materials which allows a direction dependent shifting in particular temperature regions. The overall condition is not satisfied globally for thermorheological simplicity but instead almost direction wise with acceptable deviations. The pre-defined limit of discrepancies also determines the confidence region of the allowable temperatures below and above the reference temperature. The macroscopic TTS-behaviour assembles in general from the ones of the composite's constituents for the material tensor entry $R_{1111}$ and therefore more combinations of frequent used polymers should be inspected which might result in a more universal modelling approach in terms of the macroscopic TTS behaviour.

# Appendix A

# Material input

The required material definition in ABAQUS for the fibre and matrix material is presented in section A.1 and A.2 respectively. In both definitions the code structure is similar and it is referred to the keyword manual of ABAQUS [41] for a detailed explanation.

## A.1 Material input of fibre

```
*Material, name=m_fiber
*Density
1130.,
*Elastic, Moduli=LONG TERM
1.036e+10, 0.39
*Viscoelastic, Time=Frequency data, ERRTOL=0.25, NMAX=13
0.1134388,-2.2463796,0.1134388,-2.2463796,5e-4
0.1253860,-2.2982202,0.1253860,-2.2982202,0.001
0.1575400,-2.4405170,0.1575400,-2.4405170,0.005
0.1734570,-2.5125117,0.1734570,-2.5125117,0.01
0.2156744,-2.7087652,0.2156744,-2.7087652,0.05
0.2362391,-2.8073133,0.2362391,-2.8073133,0.1
0.2897132,-3.0734790,0.2897132,-3.0734790,0.5
0.4095585,-3.7321635,0.4095585,-3.7321635,10
0.5902781,-4.9738293,0.5902781,-4.9738293,500
0.6910872,-5.9178998,0.6910872,-5.9178998,5000
0.7707515,-6.9990457,0.7707515,-6.9990457,5e4
0.8240715,-8.5409003,0.8240715,-8.5409003,1e6
0.8261093,-9.3937323,0.8261093,-9.3937323,5e6
0.8000569,-10.596268,0.8000569,-10.596268,5e7
0.7867905,-10.948048,0.7867905,-10.948048,1e8
0.7491050,-11.738294,0.7491050,-11.738294,5e8
0.7307263,-12.065578,0.7307263,-12.065578,1e9
0.6853944,-12.792126,0.6853944,-12.792126,5e9
```

```
0.6654085,-13.090198,0.6654085,-13.090198,1e10
0.6196518,-13.747862,0.6196518,-13.747862,5e10
**
*TRS, DEFINITION=WLF
313.15, 42.8, 218.6
```

## A.2 Material input of matrix

```
*Material, name=m_matrix
*Density
1200.
*Elastic, Moduli=LONG TERM
7e+08, 0.35
*Viscoelastic, Time=Frequency data, ERRTOL=0.2, NMAX=13
0.018206, 0.158499,0.0182709,0.1555,5e-12
0.0595728,-0.235515,0.0597852,-0.239919,5e-11
0.143899,-0.732198,0.144412,-0.738372,5e-10
0.238266,-1.37353,0.239115,-1.38199,5e-09
0.310416,-2.19358,0.311522,-2.20497,5e-08
0.393568,-2.95132,0.394971,-2.9654, 5e-07
0.531816,-3.62571,0.533711,-3.6422, 5e-06
0.482508,-4.06103,0.484228,-4.07907,5e-05
0.335562,-4.35475,0.336758,-4.37384,0.0005
0.232887,-4.60152,0.233717,-4.62148,0.005
0.179438,-4.83604,0.180078,-4.85684,0.05
0.13266, -5.03064,0.133133,-5.05214,0.5
0.103364,-5.1679, 0.103732,-5.18988,5.
0.103364,-5.30708,0.103732,-5.32956,50.
0.103364,-5.45935,0.103732,-5.48237,500.
0.103364,-5.55825,0.103732,-5.58163,5000.
0.103364,-5.69273,0.103732,-5.71659,50000.
0.103364,-5.79847,0.103732,-5.8227, 500000.
0.103364,-5.90477,0.103732,-5.92938,5e+06
0.103364,-6.03996,0.103732,-6.06505,5e+07
0.103364,-6.13993,0.103732,-6.16538,5e+08
0.103364,-6.26196,0.103732,-6.28784,5e+09
**
*TRS, DEFINITION=ARRHENIUS
293.15, 448e3
```

# Bibliography


[1] J. Aboudi, S. M. Arnold, and B. A. Bednarcyk. *Micromechanics of composite materials: A generalized multiscale analysis approach*. 1. ed. Amsterdam: Elsevier/Butterworth-Heinemann, 2013. ISBN: 978-0-12-397035-0. URL: http://www.loc.gov/catdir/enhancements/fy1606/2012275130-d.html.

[2] J. J. Aklonis and W. J. MacKnight. *Introduction to polymer viscoelasticity*. 3rd ed. Hoboken, N.J: Wiley-Interscience, 2005. ISBN: 9780471740452. DOI: 10.1002/0471741833. URL: http://site.ebrary.com/lib/alltitles/docDetail.action?docID=10305324.

[3] G. Akovalı, ed. *Handbook of composite fabrication*. Shawbury, U.K: Rapra Technology Ltd, 2001. ISBN: 1859572634. URL: http://site.ebrary.com/lib/academiccompletetitles/home.action.

[4] H. J. Böhm, ed. *Mechanics of Microstructured Materials*. Vol. 464. International Centre for Mechanical Sciences, Courses and Lectures. Vienna and s.l.: Springer Vienna, 2004. ISBN: 978-3-7091-2776-6. DOI: 10.1007/978-3-7091-2776-6. URL: http://dx.doi.org/10.1007/978-3-7091-2776-6.

[5] H. F. Brinson and L. C. Brinson. *Polymer Engineering Science and Viscoelasticity: An Introduction*. 2nd ed. 2015. Boston, MA and s.l.: Springer US, 2015. ISBN: 978-1-4899-7484-6. DOI: 10.1007/978-1-4899-7485-3. URL: http://dx.doi.org/10.1007/978-1-4899-7485-3.

[6] L. C. Brinson and W. G. Knauss. "Finite Element Analysis of Multiphase Viscoelastic Solids". In: *Journal of Applied Mechanics* 59.4 (1992), pp. 730–737. ISSN: 0021-8936. DOI: 10.1115/1.2894035.

[7] L. C. Brinson and W. G. Knauss. "Thermorheologically complex behavior of multiphase viscoelastic materials". In: *Journal of the Mechanics and Physics of Solids* 39.7 (1991), pp. 859–880. ISSN: 00225096. DOI: 10.1016/0022-5096(91)90009-D.

[8] L. C. Brinson and W. S. Lin. "Comparison of micromechanics methods for effective properties of multiphase viscoelastic composites". In: *Composite Structures* 41.3-4 (1998), pp. 353–367. ISSN: 02638223. DOI: 10.1016/S0263-8223(98)00019-1.

[9] K. S. Cho. *Viscoelasticity of Polymers: Theory and Numerical Algorithms*. 1st ed. 2016. Vol. 241. Springer Series in Materials Science. Dordrecht and s.l.: Springer Netherlands, 2016. ISBN: 978-94-017-7564-9. DOI: 10.1007/978-94-017-7564-9. URL: http://dx.doi.org/10.1007/978-94-017-7564-9.

[10] V. K. S. Choo. *Fundamentals of composite materials*. Dover, Del.: Knowen Academic Press, 1990. ISBN: 0929785002.

[11] D. D. L. Chung. *Composite materials: Science and applications ; [in celebration of the 20th anniversary of the composite materials research laboratory, University at Buffalo, State University of New York]*. 2. ed. Engineering Materials and Processes. London: Springer-Verlag London, 2010. ISBN: 978-1-84882-830-8. DOI: 10.1007/978-1-84882-831-5. URL: http://site.ebrary.com/lib/alltitles/docDetail.action?docID=10382676.

[12] M. H. Cohen and D. Turnbull. "Molecular Transport in Liquids and Glasses". In: *The Journal of Chemical Physics* 31.5 (1959), pp. 1164–1169. ISSN: 0021-9606. DOI: 10.1063/1.1730566.

[13] H. Domininghaus, P. Elsner, P. Eyerer, and T. Hirth, eds. *Kunststoffe: Eigenschaften und Anwendungen*. 8., neu bearb. und erw. Aufl. VDI-Buch. Berlin and Heidelberg: Springer, 2012. ISBN: 978-3-642-16172-8. DOI: 10.1007/978-3-642-16173-5. URL: http://dx.doi.org/10.1007/978-3-642-16173-5.

[14] G. Ehrenstein. *Polymer-Werkstoffe: Struktur ; Eigenschaften ; Anwendung*. 3. Aufl. s.l.: Carl Hanser Fachbuchverlag, 2011. ISBN: 978-3-446-42283-4.

[15] N Feldmann, F Bause, and B Henning. "B1. 4-Determining fractional Zener model parameters from low frequency DMA measurements". In: *Proceedings Sensor 2017* (2017), pp. 172–176.

[16] J. D. Ferry. *Viscoelastic properties of polymers*. Third edition. New York et al.: John Wiley & Sons, 1980. ISBN: 978-0-471-04894-7.

[17] P. L. Gould and Y. Feng. *Introduction to Linear Elasticity*. 4th ed. 2018. Cham: Springer International Publishing, 2018. ISBN: 978-3-319-73884-0. DOI: 10.1007/978-3-319-73885-7. URL: http://dx.doi.org/10.1007/978-3-319-73885-7.

[18] C. D. Han. *Rheology and processing of polymeric materials: Volume 1: Polymer rheology*. Oxford and New York: Oxford University Press, 2007. ISBN: 9780195187823. URL: http://lib.myilibrary.com/detail.asp?id=116265.

[19] C. A. Harper, ed. *Handbook of plastics, elastomers, and composites*. 4. ed. McGraw-Hill handbooks. New York, NY: McGraw-Hill, 2002. ISBN: 9780071384766.

[20] Z. V. Hashin. "Viscoelastic fiber reinforced materials". In: *AIAA Journal* 4.8 (1966), pp. 1411–1417. ISSN: 0001-1452. DOI: 10.2514/3.3686.

[21] Heinz E. Pettermann, Camille Cheyrou, Antonio DeSimone. *An anisotropic linear viscoelastic constitutive law: direction dependent time temperature shift functions*. 2019.

[22] D. Hull. *An introduction to composite materials*. Cambridge solid state science series. Cambridge: University Press, 1981. ISBN: 0521239915.

[23] R. M. Jones. *Mechanics of Composite Materials*. 2nd ed. Boca Raton: Chapman and Hall/CRC, 2014. ISBN: 156032712X. URL: https://ebookcentral.proquest.com/lib/gbv/detail.action?docID=5379452.

[24] K. U. Kainer, ed. *Metal matrix composites: Custom-made materials for automotive and aerospace engineering*. Weinheim and Chichester: Wiley-VCH, 2006. ISBN: 3-527-31360-5. DOI: 10.1002/3527608117. URL: http://search.ebscohost.com/login.aspx?direct=true&scope=site&db=nlebk&db=nlabk&AN=169581.

[25] K. K. Kar, ed. *Composite Materials: Processing, Applications, Characterizations*. Berlin, Heidelberg and s.l.: Springer Berlin Heidelberg, 2017. ISBN: 978-3-662-49512-4. DOI: 10.1007/978-3-662-49514-8. URL: http://dx.doi.org/10.1007/978-3-662-49514-8.

[26] L. P. Kollar and G. S. Springer. *Mechanics of composite structures*. Cambridge: Cambridge University Press, 2003. ISBN: 978-0-521-80165-2. DOI: 10.1017/CBO9780511547140. URL: https://doi.org/10.1017/CBO9780511547140.

[27] A. E. Krauklis, A. G. Akulichev, A. I. Gagani, and A. T. Echtermeyer. "Time-Temperature-Plasticization Superposition Principle: Predicting Creep of a Plasticized Epoxy". In: *Polymers* 11.11 (2019). DOI: 10.3390/polym11111848.

[28] W. Krenkel, ed. *Ceramic matrix composites: Fiber reinforced ceramics and their applications*. Weinheim: Wiley-VCH, 2008. ISBN: 978-3-527-31361-7. DOI: 10.1002/9783527622412. URL: http://search.ebscohost.com/login.aspx?direct=true&scope=site&db=nlebk&db=nlabk&AN=244361.

[29] R. S. Lakes. *Viscoelastic materials*. Cambridge: Cambridge University Press, 2009. ISBN: 9780511626722. DOI: 10.1017/CBO9780511626722. URL: https://doi.org/10.1017/CBO9780511626722.

[30] P. K. Mallick. *Fiber-reinforced composites: Materials, manufacturing, and design*. 3. ed. Boca Raton, Fla.: CRC Press, 2008. ISBN: 9780849342059. URL: http://www.loc.gov/catdir/enhancements/fy0727/2007019619-d.html.

[31] J. E. Mark. *Physical properties of polymers*. Third edition. Cambridge: Cambridge University Press, 2004. ISBN: 052182317X. DOI: 10.1017/CBO9781139165167. URL: https://doi.org/10.1017/CBO9781139165167.

[32] J. E. Mark, ed. *Physical properties of polymers handbook*. 2. ed. New York, NY: Springer Science+Business Media LLC, 2007. ISBN: 9780387312354. URL: http://dx.doi.org/10.1007/978-0-387-69002-5.

[33] MATLAB. *version 9.1 (R2016b)*. Natick, Massachusetts: The MathWorks Inc., 2016.

[34] A. H. Muliana and S. Sawant. "Responses of viscoelastic polymer composites with temperature and time dependent constituents". In: *Acta Mechanica* 204.3-4 (2009), pp. 155–173. ISSN: 0001-5970. DOI: 10.1007/s00707-008-0052-4.

[35] Nadine Feldmann. *Das Zeit-Temperatur-Superpositionsprinzip zur Messbereichserweiterung bei der Dynamisch-Mechanischen Analyse*. Ed. by Universität Paderborn. Paderborn.

[36] H. E. Pettermann and A. DeSimone. "An anisotropic linear thermo-viscoelastic constitutive law: Elastic relaxation and thermal expansion creep in the time domain". In: *Mechanics of time-dependent materials* 22.4 (2018), pp. 421–433. DOI: 10.1007/s11043-017-9364-x.

[37] M. Rubinstein and R. H. Colby. *Polymer physics*. Reprinted. Oxford: Oxford Univ. Press, 2010. ISBN: 9780198520597.

[38] H. Schürmann. *Konstruieren mit Faser-Kunststoff-Verbunden*. 2., bearbeitete und erweiterte Auflage. VDI-Buch. Berlin, Heidelberg: Springer-Verlag Berlin Heidelberg, 2007. ISBN: 978-3-540-72189-5. DOI: 10.1007/978-3-540-72190-1. URL: http://dx.doi.org/10.1007/978-3-540-72190-1.

[39] M. T. Shaw. *Introduction to Polymer Rheology*. Hoboken: John Wiley & Sons, 2012. ISBN: 9780470388440. DOI: 10.1002/9781118170229. URL: http://e-res.bis.uni-oldenburg.de/redirect.php?url=http://lib.myilibrary.com/detail.asp?id=343221.

[40] V. V. Silberschmidt. *Computational and Experimental Mechanics of Advanced Materials*. 1. Aufl. Vol. no. 514. CISM courses and lectures. s.l.: Springer Verlag Wien, 2009. ISBN: 978-3-211-99684-3. URL: http://site.ebrary.com/lib/alltitles/docDetail.action?docID=10355147.

[41] M. Smith. *ABAQUS/Standard User's Manual, Version 2018*. English. United States: Dassault Systèmes Simulia Corp, 2018.

[42] G. R. Strobl. *The physics of polymers: Concepts for understanding their structures and behavior*. 3., rev. and expanded ed. Berlin, Heidelberg: Springer, 2007. ISBN: 978-3-540-68411-4. URL: http://dx.doi.org/10.1007/978-3-540-68411-4.

[43] N. W. Tschoegl, W. G. Knauss, and I. Emri. "The Effect of Temperature and Pressure on the Mechanical Properties of Thermo- and/or Piezorheologically Simple Polymeric Materials in Thermodynamic Equilibrium – A Critical Review". In: *Mechanics of time-dependent materials* 6.1 (2002), pp. 53–99. DOI: 10.1023/A:1014421519100.

[44] I. M. Ward and J. Sweeney. *Mechanical properties of solid polymers*. 3. ed. Chichester: Wiley, 2013. ISBN: 9781444319507.

[45] W. Weißbach. *Werkstoffkunde: Strukturen, Eigenschaften, Prüfung ; mit 248 Tabellen*. 18., überarb. Aufl. Studium. Wiesbaden: Vieweg + Teubner, 2012. ISBN: 978-3-8348-1587-3. DOI: 10.1007/978-3-8348-8318-6. URL: http://dx.doi.org/10.1007/978-3-8348-8318-6.

[46] E. Witten, ed. *Handbuch Faserverbundkunststoffe/Composites: Grundlagen, Verarbeitung, Anwendungen*. 4. Auflage. Wiesbaden: Springer Vieweg, 2014. ISBN: 978-3-658-02754-4. URL: http://lib.myilibrary.com/detail.asp?id=601673.

[47] Y. T. Yeow, D. H. Morris, and H. F. Brinson. "Time-Temperature Behavior of a Unidirectional Graphite/Epoxy Composite". In: *Fifth Conference on Composite Materials: Testing and Design*. Ed. by S. W. Tsai. 100 Barr Harbor Drive, PO Box C700 West Conshohocken PA 19428-2959: ASTM International, 1979, pp. 263–263–19. ISBN: 978-0-8031-4495-8. DOI: 10.1520/STP36913S.